

# Production of Cold Molecular Radicals by Laser Ablation

Torben Müller

Blackett Laboratory  
Center for Cold Matter  
Department of Physics

Imperial College

University of London,  
London SW7 2BW,  
United Kingdom

[mueller-torben@web.de](mailto:mueller-torben@web.de)

March 2005

# Contents

<b>1</b>	<b>Introduction</b>	<b>6</b>
1.1	A generic intense source for cold molecular radicals . . . . .	6
1.2	The current technology . . . . .	6
1.3	A promising alternative and outline of the study . . . . .	8
1.3.1	YbF formation in buffer gas environment by laser ablation	8
1.3.2	Outline of the study . . . . .	8
<b>2</b>	<b>Apparatus</b>	<b>9</b>
2.1	Introduction . . . . .	9
2.2	Ablation chamber . . . . .	9
2.3	Yb Target . . . . .	11
2.4	Vacuum System . . . . .	12
2.5	Gas System . . . . .	15
2.6	Optical System . . . . .	17
2.6.1	Optical System on Laser Table . . . . .	17
2.6.2	Optical System on the Ablation Table . . . . .	19
2.7	Electronics . . . . .	24
2.7.1	Photodiode . . . . .	24
2.7.2	Divider Circuit . . . . .	26
2.8	Data Acquisition . . . . .	26
2.8.1	Hardware . . . . .	26
2.8.2	Software . . . . .	26
<b>3</b>	<b>Properties and Band Structure of YbF</b>	<b>28</b>
3.1	Chemical and Physical Properties of YbF . . . . .	28
3.2	Band Spectra of YbF . . . . .	28
3.3	Mean free path . . . . .	34
<b>4</b>	<b>Testing the Setup</b>	<b>36</b>
4.1	Yb absorption signal . . . . .	36
4.2	YbF absorption signal . . . . .	37
<b>5</b>	<b>Yb Spectrum</b>	<b>39</b>
5.1	Yb absorption spectroscopy . . . . .	39
5.2	Yb spectrum simulation . . . . .	40
<b>6</b>	<b>YbF scan near bandhead</b>	<b>43</b>

<b>7</b>	<b>Target Lifetime</b>	<b>44</b>
7.1	Current source . . . . .	44
7.2	Target Lifetime Study . . . . .	44
7.2.1	Lifetime Study without buffer gas . . . . .	45
7.2.2	Lifetime Study with buffer gas . . . . .	48
<b>8</b>	<b>Dependence of YbF Production on Buffer Gas Pressure</b>	<b>52</b>
<b>9</b>	<b>Diffusion and Transport Processes of YbF</b>	<b>56</b>
9.1	Two-dimensional diffusion study . . . . .	57
9.2	One-dimensional diffusion study . . . . .	68
<b>10</b>	<b>Production rate of YbF</b>	<b>71</b>
<b>11</b>	<b>Conclusions and outlook</b>	<b>77</b>
11.1	Conclusions . . . . .	77
11.2	Outlook . . . . .	78

## **Abstract**

This study deals with the production of molecular radicals by laser ablation. The study is performed on YbF, because it offers a high sensitivity to the electron's electric dipole moment, which is currently being measured in an experiment at Imperial College. The study tries to set a start point for a new type of molecule source that differs from that one already used in the edm and decelerator experiment at Imperial College. The new idea is to decouple the formation process of YbF from its expansion. These processes are strongly correlated in the current technology of the jet beam source for YbF which might be a limiting factor on the number of produced molecules. Additionally to that, the current source is faced with a fast decay in the flux of molecules due to a short target lifetime. Therefore, this study starts to address some of these issues.

## Acknowledgments

I would like to say thank everybody who has provided guidance, encouragement, support and friendship throughout my project. This study would not have been possible without them.

I am truly grateful to my supervisor Michael Tarbutt. From him I have learned the skills of careful planning and execution of experiments, through analysis and clear interpretation of experimental data. I am indebted to Michael for not only his advice and scientific instruction but also his good humor and patience. Especially chapter 9 of this report is his great contribution to my study. I also thank Professor Ed Hinds for the illuminating discussions during our weekly meetings.

I thank Ben Sauer for his daily help and what I have learned from him. His dedication to work and efficiency, and his rich skills and basis of experimental experiences have been a good model for me.

I have been working with Richard Darnley closely for the last six month. It has always been a pleasure to discuss some physics with him and I thank him tolerating the inconvenience of having to share the dye laser with me.

I would like to thank Jon Dyne, the mechanical technician engineer of the machine shop, for his always quick help and assistance to my apparatus design.

I have to thank for the financial support by the European Commission as being young researcher in the "Cold molecules network". Their support granted my a convenient way of working and stay in London.

I am very indebted to the "Studienstiftung des deutschen Volkes", especially to Jörn Weingärtner, who made the impossible possible and afforded my a scholarship after the deadline for its application.

Finally I am truly grateful to Professor Immanuel Bloch for his effort to enable this project in the group of Ed Hinds. Without his spontaneous engagement this work have not been possible. I cannot thank enough for his help.

# 1 Introduction

## 1.1 A generic intense source for cold molecular radicals

The production of ultracold atoms has enabled an unprecedented level of control over all the degrees of freedom at the quantum level. To achieve a comparable control over molecules requires a suitable cooling scheme.

A generic intense source for molecular radicals is expected to be useful for precision measurements using cold molecules ( e.g. electron edm, fundamental constants ), collision experiments, decelerating and trapping of molecules.

Currently, at Imperial College we are running two experiments dealing with heavy polar molecules. Firstly, an experiment to measure the electron's electric dipole moment (edm), using YbF molecules that offer a particular sensitivity to the electron's edm, and secondly, an experiment where YbF molecules are decelerated in an alternating gradient Stark decelerator.

So, the final aim of this investigation will be the development of a generic source that can be useful for these two experiments mentioned above, but also for other applications, since its character shall be generic. This study is meant to be the first step towards this new source, dealing with the production process of cold molecular radicals by laser ablation.

## 1.2 The current technology

As already mentioned in the first section, at Imperial College we are running two experiments working with heavy polar molecules. The fundamental basis of the edm experiment is the fact that heavy, paramagnetic polar molecules provide a much higher sensitivity to the electron's edm than for example atoms do, such as Cs or Tl. From a wide range of such molecules YbF emerged the most promising candidate. The selection process for YbF is discussed in the thesis of Jun Wang [1]. For that reason, this study will especially concentrate on the production of YbF by laser ablation.

Before going into details I would like to present the current technology of the molecule source that is already used in the edm and the decelerator experiment. Both experiments utilize a jet beam source of cold YbF radicals [2]. Figure 1 shows the schema of this source.

To summarize the important facts about this technique, cold YbF molecules are formed by ablating an Yb target using a pulsed YAG laser and entraining

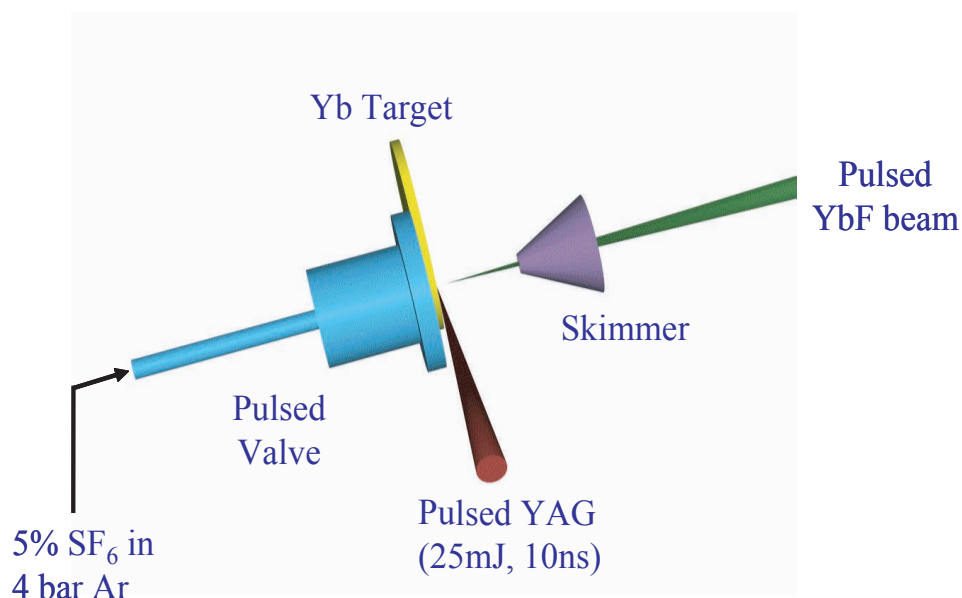


Figure 1: Current technology of a supersonic beam source for cold YbF radicals

the Yb in a supersonically expanding jet of argon, containing a small fraction of SF<sub>6</sub>. Via collisions the Yb reacts with the SF<sub>6</sub> to YbF which has a radical character. The resulting pulses of YbF have translational and rotational temperatures of about 3 K. Each pulse contains about  $1.4 \cdot 10^9$  molecules per steradian in the X<sup>2</sup>Σ<sup>+</sup>( $\nu = 0, N = 0$ ) ground-state. The vibrational temperature is such that at least 98% of the molecules are in the ground vibrational state. The translational and rotational temperatures of the beam are equal.

However, in order to improve the sensitivity of those experiments which use this source, there are mainly three points of interests this study will focus on:

- a higher number of produced molecular radicals
- a better shot-to-shot stability
- an extension of the target lifetime

## **1.3 A promising alternative and outline of the study**

### **1.3.1 YbF formation in buffer gas environment by laser ablation**

In the current source the production of molecular radicals by laser ablation and the supersonic expansion are strongly correlated, i.e. the timing between the opening of the pulsed valve and the firing of the YAG, and the transverse position of the target need to be carefully controlled. This requirement might be a limitation especially for the number of produced YbF molecules.

In order to decouple these two processes, a buffer gas (cooled) source for molecules is expected to be a promising alternative. The idea is to form molecular radicals by ablating a target inside a buffer gas cell. The formation process of molecules, e.g. YbF, can be implemented either by ablating solid precursors or by ablating a Yb target and adding a small fraction of fluorine containing gas to the buffer.

For that reason, this study will concentrate on the production process of YbF by laser ablation of Yb inside a buffer gas environment (Ar/SF<sub>6</sub>), instead of entraining the ablated Yb in an expanding pulse of buffer gas. We are hoping that this new assembly offers a chance to fulfill the points of interests as mentioned above. So, the task is to study the formation of molecular radicals in this setup under certain conditions, such as buffer gas pressure and energy in the ablation pulse with respect to the number of produced radicals and target lifetime.

### **1.3.2 Outline of the study**

The following chapters of this study are organized as below:

In chapter 2, the experimental apparatus is described, together with the program used for data acquisition. This chapter might be quite extended, but should be useful for those who are going to continue this study towards a generic source for cold molecular radicals.

In chapter 3, we summarize some chemical and physical information about Yb and YbF, which is mainly adapted from the thesis of Jun Wang [1].

In the following chapters we will discuss some of the results obtained during the last six month of this study, such as the target lifetime, the dependence of YbF formation on buffer gas pressure, the diffusion processes of YbF in the ablation cell and finally an estimation of the order of magnitude of produced YbF in the vibrational and rotational ground-state.

## 2 Apparatus

### 2.1 Introduction

In this chapter, we will give a short introduction to the apparatus that was used for the study of the production processes of YbF. It contains all the information about the ablation cell itself, about the gas and vacuum systems, the lasers used for ablation and probing and the data acquisition. At some points we will discuss the modifications and improvements made during the last six months and will always refer to that stage of the setup which was used for a particular measurement. The scale of this chapter was wittingly chosen being described in detail, so that those, who will continue the study, get an informative overview on the apparatus.

### 2.2 Ablation chamber

As mentioned before, producing YbF molecules in a buffer gas cell is expected to be a promising alternative. The buffer gas cell used in these experiments is shown in Figure 2. The cell consists of a simple 6-way-cross made of stainless steel (Caburn MDC: KX6-50).

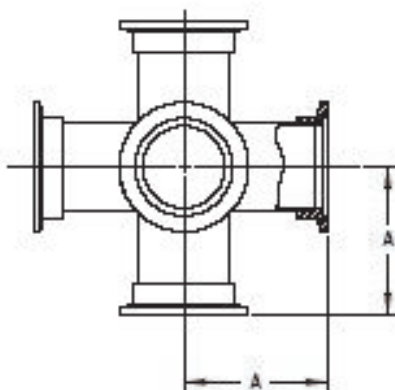


Figure 2: 6-way-cross used as ablation cell ( $A = 50\text{mm}$ )

A pulsed YAG laser strikes a Yb target sitting in the middle of the gas chamber. Thus, the center of the six-way cross is where YbF molecules are produced, and also where these radicals interact with the probe laser beam (see Figure 3).

The YAG laser pulses enter the reaction chamber through one arm of the cross and go straight on towards the Yb target mounted on an aluminium rod, which is fixed in a screw socket in the opposite arm. During the first time of measurements

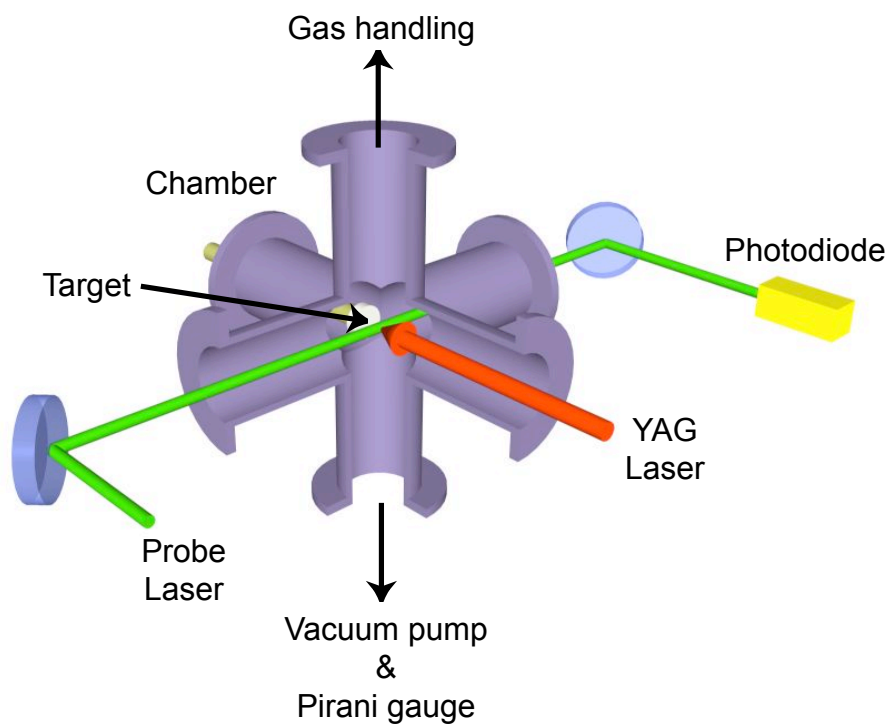


Figure 3: Ablation cell

the window, the YAG light passes through, was just a round pane of simple glass glued into the flange of the chamber arm with "Torr Seal". But because this window was accidentally damaged by the YAG, we decided to replace this construction by a prefabricated window tube piece with tinted glass (Lesker viewport QF25) that is connected to the 6-way-cross with a hinged clamp in order to replace it easily in case of damage.

The probe laser beam passes the cell and the reaction zone perpendicular to the pulsed YAG beam so that both beams lie in a horizontal plane. For the probe beam we maintained the glued in windows in the other axis of the 6-way cross, because the probe beam is not supposed to do harm to the windows.

The top flange of the 6-way-cross is connected to the gas system, the bottom flange leads to the vacuum system and the pressure gauge.

All stainless steel vacuum fittings and components of the setup ordered from the Caburn-MDC KF Kwik-Flange series are assembled with an O-ring and a hinged clamp. Each seal is made by compression of an O-ring on a centering ring between mating flanges by finger-closure of a wingnut on the all-metal hinged aluminium clamp (see Figure 4).

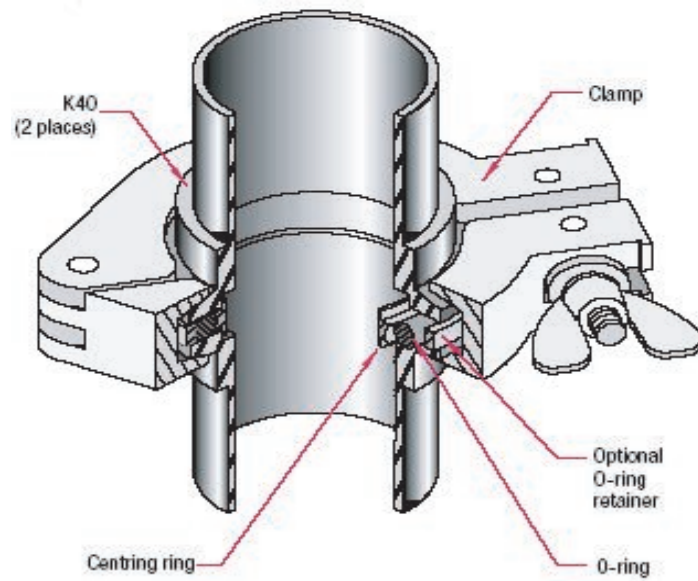


Figure 4: Hinged clamp assembly

### 2.3 Yb Target

The ablation target itself is a small piece of pure Yb metal (99,9% purity). The typical dimensions of the Yb targets we used are 4 x 8 mm with a mean thickness of 1.5 mm - 2 mm. We utilized a couple of targets, just to be able to change them quickly, if it was necessary. But all targets came from the same charge. Before involving them in the experiment that surface, which was chosen to be ablated, was polished with a fine file and then rinsed off with methanol. We always applied this cleaning process just before a target was assembled into the ablation cell.

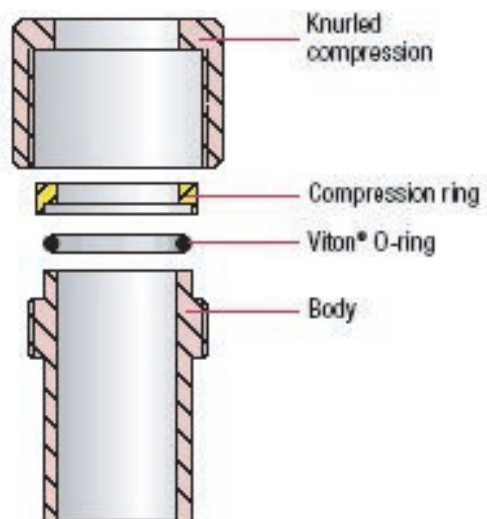


Figure 5: Quick-disconnect adapter

The target is glued on a cylindrical aluminium rod with "Torr Seal" (diameter: 0.25", length:  $\sim 10$ "). The rod itself is clamped by a Caburn-MDC Flanged Quick Disconnect (see Figure 5), which provides a fast and convenient method for coupling and uncoupling metal tubing and rods. This connector is mated via an adapter (40mm to 30mm flange, Caburn-MDC: KST-25-16) to the the cell flange opposite the YAG support. Thus, that special fitting permits a speedy change of the target's horizontal position in the cell.

## 2.4 Vacuum System

Since this study deals with the formation of molecular radicals in a buffer gas environment we like to avoid any influence of atmosphere gas. But on the other hand we are working with buffer gas at a certain pressure. Thus, it is entirely adequate having the possibility to pump the cell down to rough vacuum. For that purpose we use a rough vacuum pump (Balzers PK D31 702) with a minimum pressure level at about 100 micron.

As already mentioned the vacuum output sat on top of the 6-way-cross. It is implemented by a blank 40mm flange with a 0.2" hole, where a 0.25" aluminium pipe (length:  $\sim 10$ ") is welded on.

Figure 7 shows one of the first vacuum systems we were working with. Here

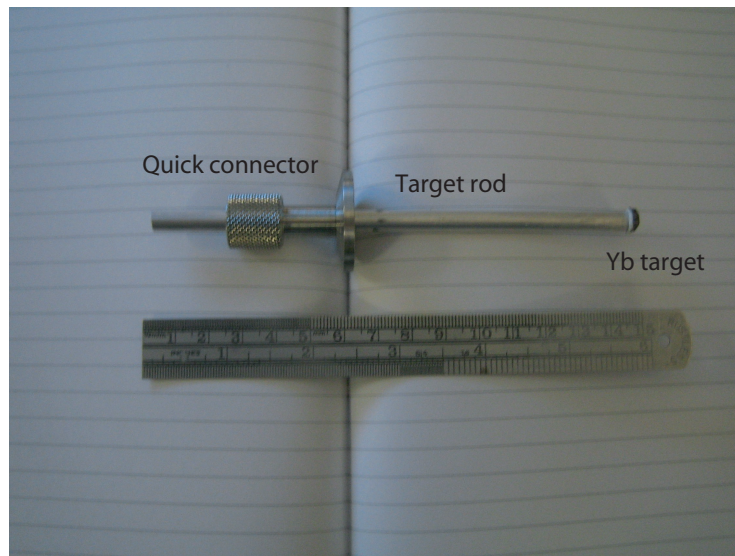


Figure 6: Yb target on aluminium rod

the vacuum and the gas system still shared one support to the 6-way-cross.

Running with this setup, we soon realized that it is more reasonable to decouple both system and separate them spatially in order to have a better control over the pressure inside the cell. Thus, now the top flange of the 6-way-cross is connected to the gas system, whereas the bottom flange leads to the vacuum system and the pressure gauge (see Figure 8).

We tried a couple of types of vacuum valves and it turned out that a combination of a simple tap and a needle valve provides a convenient control over the vacuum parameters. Figure 8 shows the very recent setup of our vacuum system. Additionally to that, we used a bypass system with another tap going round the vacuum needle valve permitting a speedy evacuation of the buffer gas cell since the needle valve drastically slows the pump velocity down.

As mentioned above, the bottom flange of the gas chamber also goes to a pressure gauge. Actually, the bottom flange is connected to a 4-way-cross (Caburn-MDC: KX4-25) via a 90° elbow (Caburn-MDC: KL-25). One arm of the 4-way-cross leads to the vacuum pump output, the other one is just sealed with a blank flange and the third one is mated to a Pirani pressure gauge (Leybold R221) via a reducer fitting (40mm to 30mm flange , Caburn-MDC: KST-25-16).

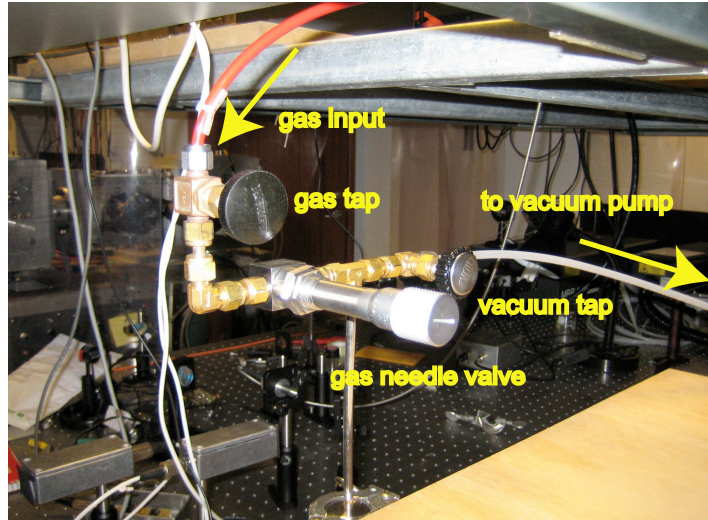


Figure 7: Combined vacuum and gas system

Note: Since we utilize a mechanical vacuum pump for evacuating the cell down to rough vacuum we are faced with undesirable pump oil in the vacuum system and even in the ablation chamber. We noticed this effect especially when we used no buffer in the cell while firing with YAG onto the target. In that case we could observe a black layer on the target surface which might be due to any carbonized component of the pump oil. Therefore, we assembled a trap for pump oil between the vacuum pump and the vacuum valve system at the buffer gas cell. In fact, it turned out that a system of a cold trap and an absorption trap is most efficient to avoid pump oil effects.

The cold trap simply consists of a copper pipe coil as an intermediate part of the vacuum pipe running through liquid nitrogen. If pump oil comes up the vacuum pipe towards the 6-way-cross, it will be frozen out in the copper coil (see Figure 9).

The absorption trap is a cylindrical container filled with an absorbing material, in our case just stainless steel wool, which effectively prevents the back-streaming of hydrocarbons from the roughing pump (see Figure 10). The gas stream of the vacuum pump runs through this container.

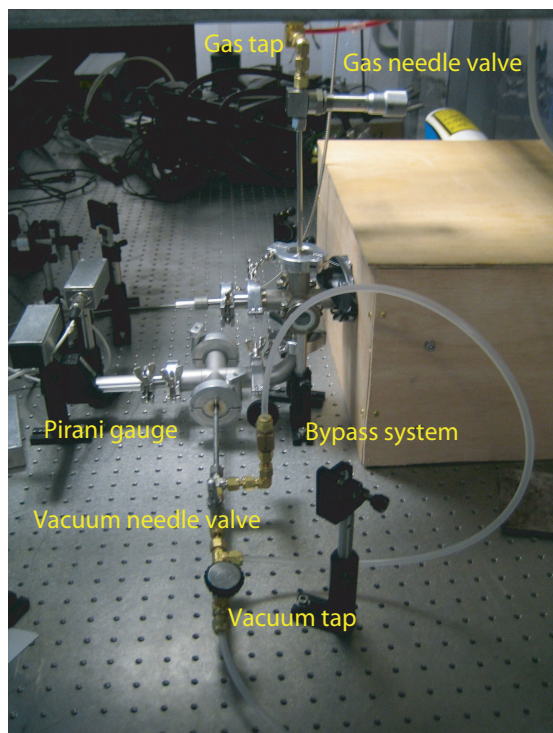


Figure 8: Combined vacuum and gas system

## 2.5 Gas System

As buffer gas we used Ar with a small fraction of  $\text{SF}_6$  (2%). The buffer can be purchased ready mixed with an accuracy of 20% for the  $\text{SF}_6$  fraction.

The gas system simply consists of a connecting 0.25" plastic tube between the gas bottle and a system including a gas tap and a needle valve sitting on top of the aluminium pipe with the blank flange, as described in the previous subsection (see Figure 8).

Having separated the gas and vacuum system we are able to control the pressure inside the cell according to the accuracy of the pressure gauge and to keep a constant flux of buffer gas through the reaction zone which we consider to be necessary in order to have always a sufficient amount of fluorine containing gas in the reaction zone for the formation of YbF.

Gas system and vacuum system pipes and tubes are connected to each other with SWAGELOK tube fittings.

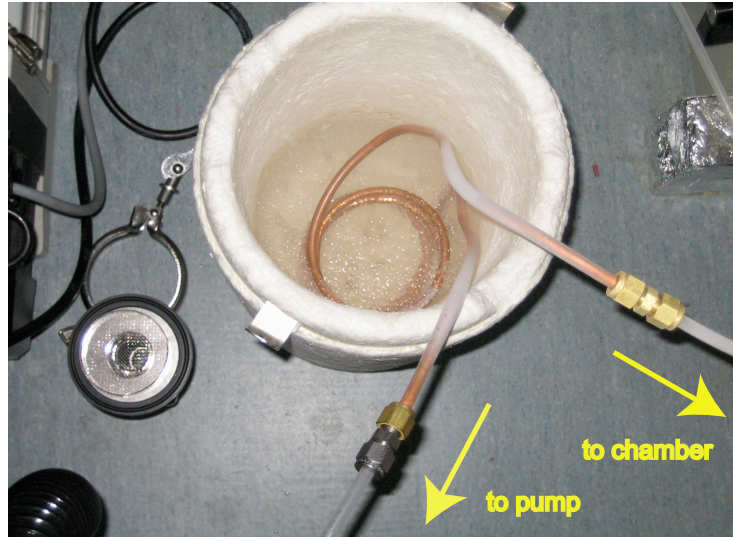


Figure 9: Cold trap for pump oil running through liquid nitrogen



Figure 10: Absorption trap for pump oil

## 2.6 Optical System

The optical components used for the presented experiment are mainly separated on two tables. There is a laser table where the probe beam for the absorption study is generated and controlled with respect to power and frequency, and another table, the so-called ablation table, where the ablation experiment itself is located.

### 2.6.1 Optical System on Laser Table

**Dye Laser** Figure 11 shows the optical system on the laser table. A "Coherent Inc. Innova 310C" argon ion laser running on multi line power (457-514 nm) is used to pump a "Coherent 899-21" ring dye laser. The dye used is Rhodamine 110. With 6W of pump power, the single mode cw output power of the dye laser is typically 300 mW at 552 nm when the dye is fresh. The R110 dye degrades after 250 Watt-hours of use and needs to be replaced about every month.

**Wave Meter** The wave meter we are using for frequency scanning of the dye laser is based on the principle of a Michelson interferometer. It has two arms which detect the interference fringes produced by the light of unknown wavelength and by the light from a temperature stabilized He-Ne laser built into the wave meter. These fringes are produced as follows. The light is first split into two beams, which are sent, via separate paths, to two corner cubes housed in a moving cart. After having been reflected by the two corner cubes, the two beams are recombined on a photodiode. When the cart travels back and forth on its track, the optical path difference between the two split beams changes, thus the fringes. The wave meter circuitry compares the number of fringes by the unknown light with that from the He-Ne laser, whose wavelength is known. And from the ratio of these two numbers, it determines the unknown wavelength. This wave meter has an accuracy of 0.0001 nm, which is about 100 MHz for our wavelength.

**Probe Laser Beam** The dye laser provides the probe beam for the presented ablation experiment and is also used for the decelerator experiment. A small fraction of the laser power is used for the ablation experiment. This beam is directly coupled, via a beam splitter and a mirror into an optical fiber. Figure 11 is simplified and does not show all optical elements on the laser table. The setup of these optical elements often changes with respect to the running decelerator experiment. The power of the probe laser beam for the ablation experiment on the fiber input usually lies in the order of magnitude of 30 mW to 60 mW, i.e. 10% to 20% of the dye laser output. However, we do not need more than 1-2 mW probe beam power for the absorption study. As it will be later described, we are able to control the probe beam power with an attenuator on the ablation table.

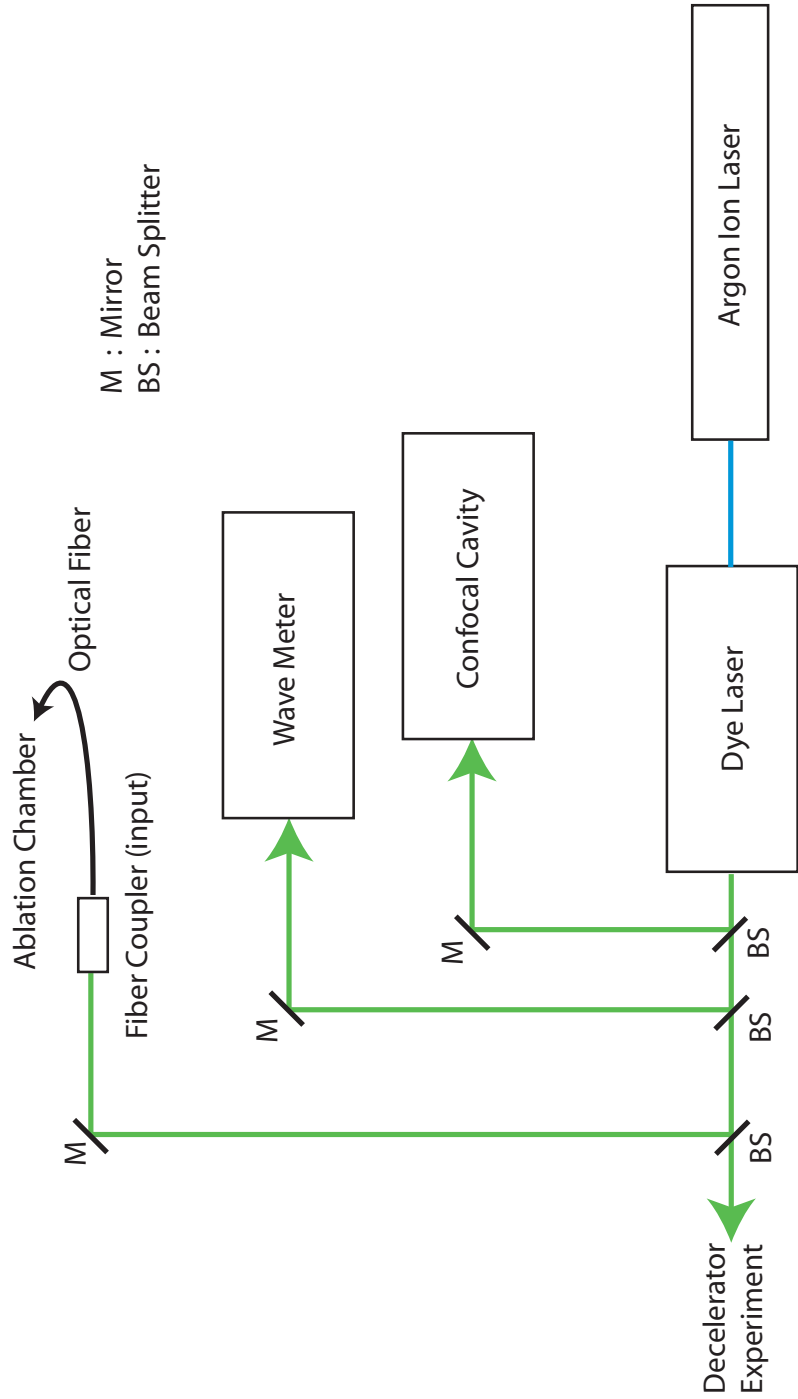


Figure 11: Optical system on laser table

The laser frequency scan is not linear, particularly near both ends of the voltage ramp driving the "Coherent 899-21" ring dye laser. In order to correct for this non-linearity, we use a confocal Fabry-Perot cavity, whose interference fringes are used as frequency markers for the laser scan. The free spectral range for this cavity is

$$FSR = \frac{c}{4r} = 250MHz \quad (1)$$

where  $r$  is the mirror's radius of curvature. With the intensity reflectivity  $R$  of the mirrors at 550nm the finesse is given by

$$F = \frac{\pi\sqrt{R}}{2(1-R)} = 2 \rightarrow 3 \quad (2)$$

**Fiber Optics** The fiber optic is used to transport light from the decelerator/laser table to the ablation cell on another table. This allows us to adjust the laser and other components on the laser table without disturbing the position of the output beam at the buffer gas chamber. Additionally, the optical fiber also serves as a spatial filter, producing clean Gaussian output beam. In our case we use a 8m long "Point Source" polarization preserving fiber. This fiber transmits a linear and stable state of polarization if two conditions are satisfied. Firstly, the input polarization must be linear and stable, and secondly, the input state of polarization must be aligned to the "birefringence" axes of the fiber. If the latter condition is not satisfied, the output polarization may drift between elliptical and linear polarization as the fiber cable is heated or mechanically disturbed.

Without any focussing onto the fiber input we achieve a transmission of 30% to 50% through the fiber.

The fiber goes through a cable duct on the lab ceiling to the ablation table. Later on, we fixed the fiber with elastic bands on the ceiling, because we guess that the fiber picks up mechanical vibrations from the air conditioning and other devices in the lab.

### 2.6.2 Optical System on the Ablation Table

Figure 12 shows the setup on the ablation table. Coming out of the fiber the probe beam passes the ablation cell through two windows and is finally detected by a photodiode. The fiber output itself can be moved horizontally and vertically, also all mirrors M1 - M3. Thus, we have a good control over the probe beam's position in the cell, e.g. we can change its horizontal position so that it is still parallel to the optical table plane. M3 serves to point the probe beam on the photodiode. The attenuator provides a good control over the intensity of the probe beam. The

function of the reference photodiode will be discussed in the next section. The prism allows us to change the position of the YAG light pulses striking the Yb target inside the cell. There is no particular reason for using a prism instead of a mirror apart from the fact that there was no YAG mirror available at the time we set up the experiment. Since we are studying the behavior of that molecule source with respect to several parameters, the energy in the ablation pulse is one point of interest as a critical parameter. Therefore, a focussing lens is used to change the energy per unit area.

**YAG Laser** As mentioned in the first section we are studying the formation of molecular radicals by laser ablation. In the the presented study we used a pulsed Nd:YAG Q-switched laser ("Quantel brilliant"). The active medium is a Nd:YAG rod optically pulse-pumped by a flashlamp at 20 Hz. The following table summarizes some important characteristics about the "Quantel brilliant":

Principal radiations	1064 nm	532 nm	216 nm
Max. energy/pulse	400 mJ	200 mJ	50 mJ
Max average power	8 W	4 W	1 W
Pulse duration	5 ns	4 ns	4 ns

By adjusting the time delay between flashlamp and the Q-switch triggers we are able to control the output energy of the YAG laser. In order to get the correlation between flashlamp/Q-switch delay time and YAG power for the 1064 nm radiation we measured it as follows in Figure 13:

The size error bars due to the power meter's uncertainty changes with the power meter's scale used while measuring a particular value. There are no error bars for the delay time, because the error is supposed to be smaller than it can be illustrated. Although having used a de-focussing lens in order not exceed the maximum of the power meter ( $0.6 \text{ J/cm}^2$ ), nearly nothing of the YAG pulses got lost, but the entire light reached the active area of the power meter.

The data clearly show the same behavior as the data taken with a photodiode, where we put a PD outside the YAG box close to a small aperture in the box and measured the PD signal for different flashlamp/Q-switch delay times.

Thus, this calibration curves can be supposed to describe the correlation between flashlamp/Q-switch delay time properly in the range between  $220 \mu\text{s}$  and  $450 \mu\text{s}$  delay time. Obviously, there is a linear relationship between delay time and YAG power in the range of  $220 \mu\text{s}$  and  $340 \mu\text{s}$ , where we are going to run the YAG laser.

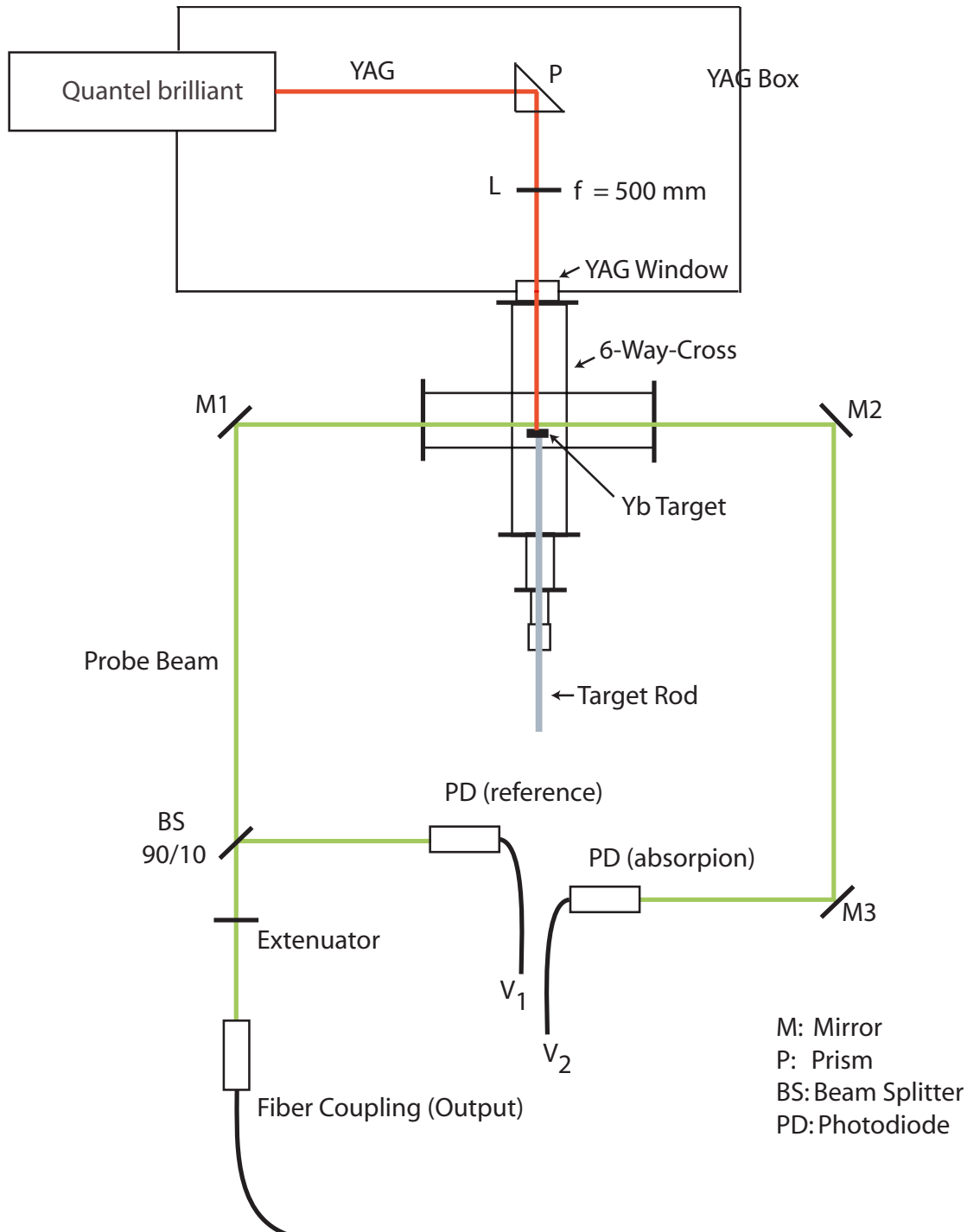


Figure 12: Optical system on the ablation table

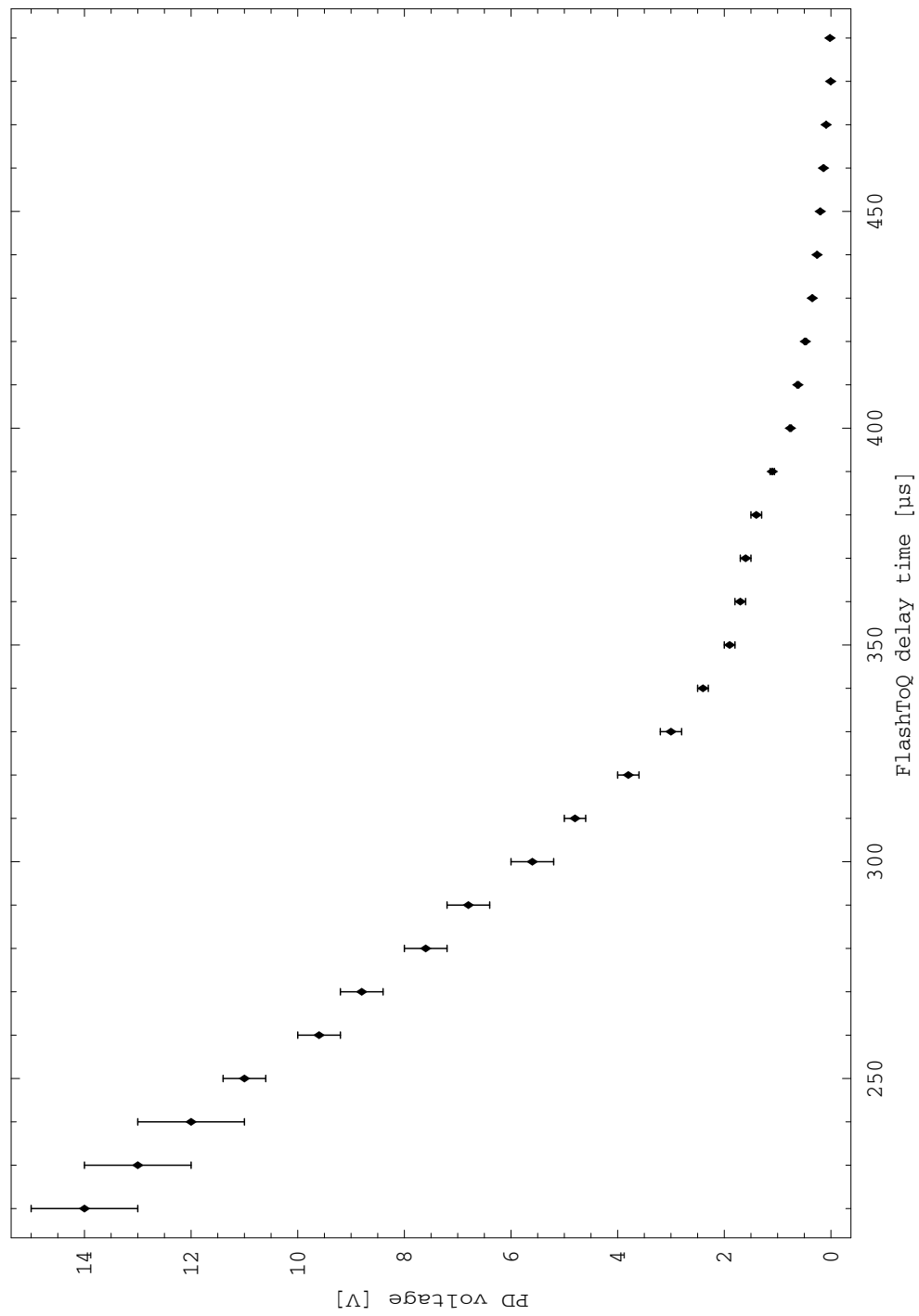


Figure 13: Correlation between YAG power and flashlamp/Q-switch delay time

Since this Quantel brilliant YAG laser was on repair for the first time of data acquisition, i.e. from December 2004 to 11/01/2005, we used another YAG laser on loan, a "Quantel brilliant b" with different characteristics:

Principal radiations	1064nm
Max. energy/pulse	900 mJ
Max average power	9 W
Pulse duration	6 ns

Flash/Q delay time [ $\mu$ s]	energy [mJ]	Flash/Q delay time [ $\mu$ s]	energy [mJ]
233	870-880	340	360
240	830	350	315-320
250	760-770	360	270-275
260	685	370	255-260
270	600	380	230
280	530	390	215
290	460-470	400	210
300	415-420	410	200
310	395-400	420	190
320	390	430	185
330	385	above 440	no signal

The "Quantel brilliant b" YAG laser was only used for the Yb-spectroscopy. In that case we run it with a delay time of 430  $\mu$ s, i.e. in its lowest energy mode at 185 mJ per pulse.

In the following it will be clearly said which data were taken with the according YAG laser.

## 2.7 Electronics

### 2.7.1 Photodiode

We are studying the formation of YbF by observing the absorption signal of a probe beam passing through the reaction zone in the ablation cell. In order to detect the absorption signal we shine the probe beam light on a photodiode. Figure 14 shows the photodiode circuit. The output voltage is proportional to the current through the photodiode.

$$V_{out} = R_i \cdot I_{PD} \quad (3)$$

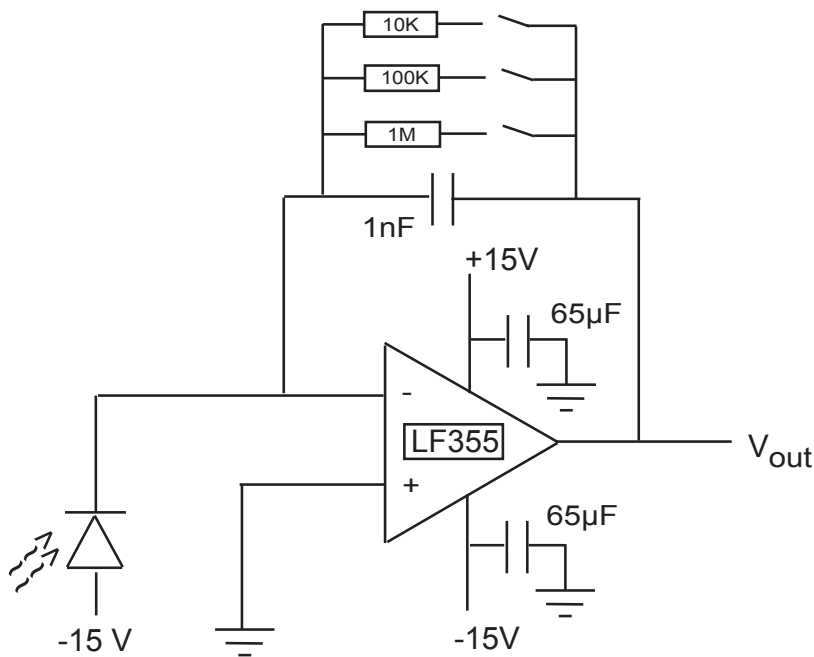


Figure 14: Photodiode Circuit

The capacitors for the  $\pm 15$  V power supply were added subsequently, because the photodiode was ringing at about 6 kHz.

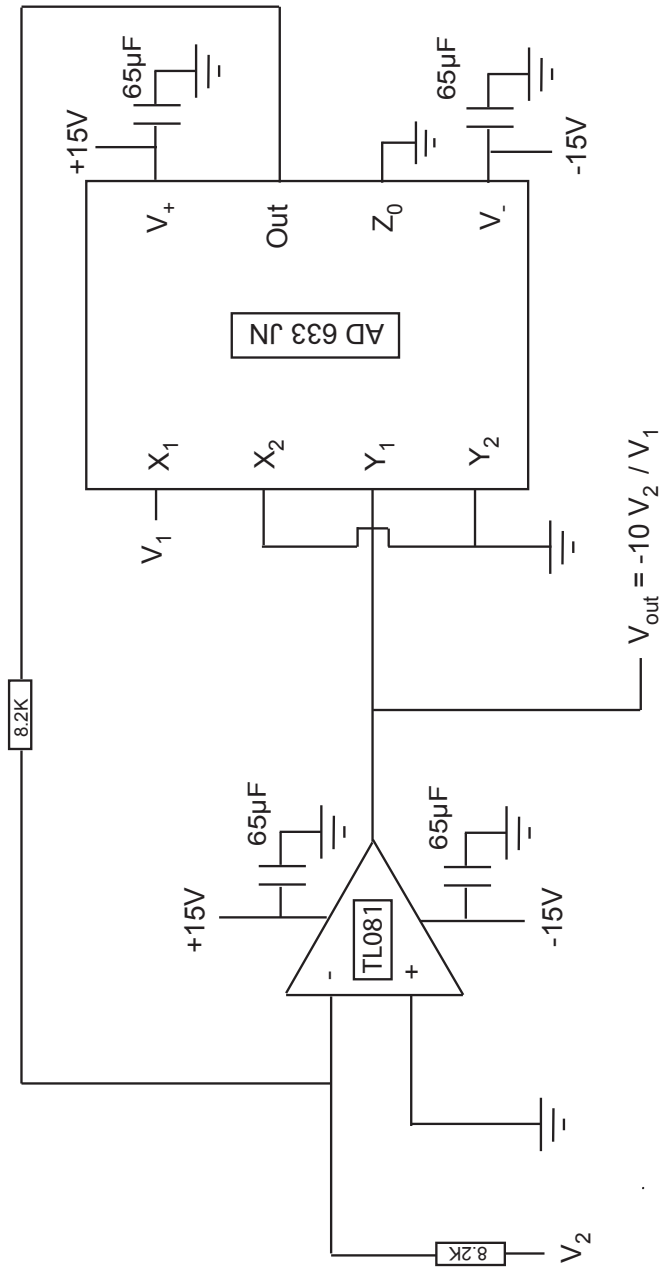


Figure 15: Analog Divider Circuit

### 2.7.2 Divider Circuit

Since the coupling of the dye laser light depends on its frequency the intensity at the fiber output changes while scanning the frequency. These intensity fluctuation causes a slightly increase of the detected absorption signal. In order to compensate this increase we use an additional photodiode that detects a part of the probe beam light before it passes through the ablation cell. A beam splitter in front of M1 provides the light for this reference photodiode. With the analog divider circuit shown in Figure 15 we divide the absorption signal  $V_2$  by the reference signal  $V_1$ .

$$V_{out} = -10 \cdot \frac{V_2}{V_1} \quad (4)$$

This divider circuit was used whenever the probe beam frequency was scanned during a measurement, i.e. for absorption spectroscopy.

## 2.8 Data Acquisition

### 2.8.1 Hardware

A PC was used to collect all the experimental data and to analyze it. Two commercial data acquisition boards from National Instruments (PCI 6534 and PCI - 6251) provided the interfaces between the computer and the experiment.

### 2.8.2 Software

The data program "ScanMaster" written by J.J Hudson and M.R. Tarbutt was used to control the experiment and to acquire the data. This program offers the possibility to control - among other parameters- the frequency scan of the dye laser (scan width) and the power of the YAG laser by varying the flashlamp/Q-switch delay time. It starts the laser scan and the YAG pulses and stores the absorption signal detected by the two photodiodes each time the YAG has stroked the Yb target. We usually choose a detecting time of 2 ms to 10 ms that is triggered by the signal for the Q-switch. Since the YAG fires at 20 Hz (fixed value that cannot be changed) we get 50 absorption profiles per second. Additionally to that, the program integrates over each of these absorption profiles. Thus, while the probe laser frequency is scanned we get a spectrum out of these integrated absorption profiles. The absorption profiles and spectrum are simultaneously displayed on the computer screen. The laser frequency scan can be repeated as many times as necessary to achieve an acceptable signal to noise ratio. When we do absorption

spectroscopy, we usually take the divided signal  $V_{out} = -10 \cdot V_{ref} / V_{abs}$  in order to avoid the intensity drift as described in the previous section.

## 3 Properties and Band Structure of YbF

### 3.1 Chemical and Physical Properties of YbF

Yb exists naturally as a mixture of seven stable isotopes:  $^{168}\text{Yb}$  (0.13%),  $^{170}\text{Yb}$  (3.05%),  $^{171}\text{Yb}$  (14.3%),  $^{172}\text{Yb}$  (21.9%),  $^{174}\text{Yb}$  (31.8%) and  $^{176}\text{Yb}$  (12.7%). Since we use natural Yb we form all seven isotopomers of YbF. YbF is highly ionic. One electron is transferred from Yb to F, leaving two closed-shell ions and a single electron localized on Yb and predominantly having the Yb  $6s\sigma$  character. The unpaired electron makes YbF paramagnetic (hence suitable for the electron EDM measurement), but it also makes the molecule highly reactive and therefore difficult to work with.

### 3.2 Band Spectra of YbF

In this subsection we give a short introduction and overview on the 0-0 band of the  $A^2\Pi_{1/2} - X^2\Sigma^+(\nu = 0)$  state of YbF.

As summarized in the paragraph above, Yb has a filled 4f shell and two valence electrons in the 6s orbital. For that reason, its electronic configuration can be represented by  $[\text{Xe}]4f^{14}6s^2$ . When forming YbF, one 6s electron of Yb is transferred to F while the other one remains localized on Yb and still predominantly has the 6s character. Therefore, to a good approximation, YbF consists of a metal-centered electron outside a core which includes two closed-shell ions  $\text{Yb}^{2+}$  and  $\text{F}^-$ . due to this alkali-atom like structure, the ground and the first states of YbF are mainly determined by the state of the unpaired electron.

The ground state X is a  $^2\Sigma^+$  state because the unpaired Yb 6s electron has a spin  $\vec{S}$  with  $S = 1/2$  and an orbital angular momentum  $\vec{L}$  with  $\Lambda = 0$ . The + sign refers to the symmetry with respect to reflection in the plane containing the internuclear axis. Other than the electronic motion, a diatomic molecule like YbF has two additional modes of motion which do not occur in atoms: the two atoms in the molecule can vibrate along the internuclear axis and the molecule can rotate as a whole about an axis passing through the molecule's center of gravity and perpendicular to the internuclear axis. The bulk of energy structure for the vibrational and rotational energy levels is shown in Figure ?? and given by

$$G(\nu) = \omega_e(\nu + \frac{1}{2}) - \omega_e x_e(\nu + \frac{1}{2})^2 + \omega_e y_e(\nu + \frac{1}{2})^3 + \dots \quad (5)$$

$$F_\nu(N) = B_\nu N(N+1) - D_\nu N^2(N+1)^2 + \dots \quad (6)$$

where  $\nu$  is the vibrational quantum number,  $N$  is the rotational quantum number, and the other symbols are constants of the molecule determined from spectroscopic measurements.

However, equation (6) does not include the interaction  $\gamma\vec{S} \cdot \vec{N}$  between  $\vec{S}$  and the molecular rotation  $\vec{N}$ . When this is taken into consideration, one rotational level is split into two which are characterized by the quantum number  $J$  of the total angular momentum  $\vec{J} = \vec{S} + \vec{N}$ . Explicitly, these two levels are given by

$$F_1(N) = B_\nu N(N+1) - D_\nu N^2(N+1)^2 + \frac{1}{2}\gamma N, J = N + \frac{1}{2} \quad (7)$$

$$F_2(N) = B_\nu N(N+1) - D_\nu N^2(N+1)^2 - \frac{1}{2}\gamma(N+1), J = N - \frac{1}{2} \quad (8)$$

The first excited state of YbF is a  $^2\Pi$  state (the unpaired electron is well described by the atomic orbitals centered on Yb, partially in the 5d and partially in the 6p states). Due to the large fine structure interaction  $A\Lambda\Sigma$ , two terms  $A_1$  and  $A_2$  with total angular momenta  $\Omega = 1/2(\Lambda = 1, \Sigma = -1/2)$  and  $\Omega = 3/2(\Lambda = 1, \Sigma = 1/2)$  respectively are formed, with the  $A_2$  well above  $A_1$  because  $A > 0$ . Only the  $A_1$  term is involved in the experiments presented here, so we will only concentrate on  $A_1$  and will just call it the A state from now on. In this state,  $\vec{\Omega}$  and  $\vec{N}$  combine to give the total angular momentum  $\vec{J}$ . This angular momentum coupling scheme is known as Hund's case (a). Since  $\vec{\Omega}$  and  $\vec{N}$  are perpendicular to each other,  $\vec{J}^2 = \vec{\Omega}^2 + \vec{N}^2$ . Thus, omitting  $\vec{\Omega}^2$  which is a constant for a given electronic term, we can replace  $\vec{N}^2 = N(N+1)$  with  $\vec{J}^2 = J(J+1)$  in the energy expressions of the rotational levels and get

$$F_\nu(NJ) = B_\nu J(J+1) - D_\nu J^2(J+1)^2 + \dots \quad (9)$$

$J$  cannot be smaller than its component  $\Omega$  or  $N$ , therefore we have

$$J = \Omega, \Omega + 1, \Omega + 2, \dots = \frac{1}{2}, \frac{3}{2}, \frac{5}{2}, \dots \quad (10)$$

corresponding to  $N = 0, 1, 2, \dots$ . Every energy level given by equation (9) is doubly degenerated because of the two relative orientations of  $\vec{\Omega}$  with respect to the internuclear axis.

The above discussion is based on the presumption that  $\vec{L} + \vec{S}$  is strongly coupled to the internuclear axis so that energy is independent of the sign of their projection  $\Omega$ . However, with increasing rotation, the coupling between  $\vec{L}$  and  $\vec{N}$

becomes appreciable and the degeneracy with respect to  $\Omega$  is lifted. The resulting eigenstates are the symmetric and anti-symmetric combinations:

$$\phi_e = \frac{1}{\sqrt{2}} \left[ \left| \Omega = +\frac{1}{2} \right\rangle + \left| \Omega = -\frac{1}{2} \right\rangle \right] \quad (11)$$

$$\phi_f = \frac{1}{\sqrt{2}} \left[ \left| \Omega = +\frac{1}{2} \right\rangle - \left| \Omega = -\frac{1}{2} \right\rangle \right] \quad (12)$$

This phenomenon is called the  $\Lambda$ -doubling. Explicitly, the energies are given by

$$F_e(J) = B_\nu J(J+1) - D_\nu J^2(J+1)^2 - \frac{1}{2}p(J + \frac{1}{2}) \quad (13)$$

$$F_f(J) = B_\nu J(J+1) - D_\nu J^2(J+1)^2 + \frac{1}{2}p(J + \frac{1}{2}) \quad (14)$$

where  $p$  is the  $\Lambda$ -doubling constant and is related to the strength of the  $\vec{L} \cdot \vec{N}$  interaction. The parity of the symmetric e-state is given by  $(-1)^{J+1/2}$  and that of the anti-symmetric f-state is given by  $(-1)^{J+1/2}$ .

The allowed transitions between the ground vibrational levels of X and A, i.e.  $\nu = \nu' = 0$ , are those allowed by the electric dipole selection rules:

- odd parity  $\leftrightarrow$  even parity
- $\Delta J = J' - J = 0, \pm 1$ , where  $J'$  and  $J$  are the total angular momenta of the upper and lower levels respectively.

They can be grouped into 6 categories or branches as shown in Figure 16. In the notation for the transitions, the main symbol P, Q or R represents  $\Delta J = -1, 0$  or  $+1$ . The superscript symbol O, P or Q represents  $\Delta J = N' - N = -2, -1$  or  $0$ , where  $N'$  and  $N$  are the rotational quantum numbers of the upper and the lower levels respectively. This superscript is omitted when  $\Delta J = \Delta N$ . The subscript "1" is abbreviated from "11", where the first "1" reminds us that the upper electronic state is really  $A_1$  although we have noted it as A., while the second "1" means that the level is  $F_1$  of the X state. When the lower level is  $F_2$ , the subscript is "12". The transitions are indexed with  $N$  of the lower level, e.g. the first line in Figure 16 is  ${}^O P_{12}(2)$ . Because in the upper state, the two components  $F_e$  and  $F_f$  of the  $\Lambda$ -doublet have opposite parities, only one of them can have transitions to

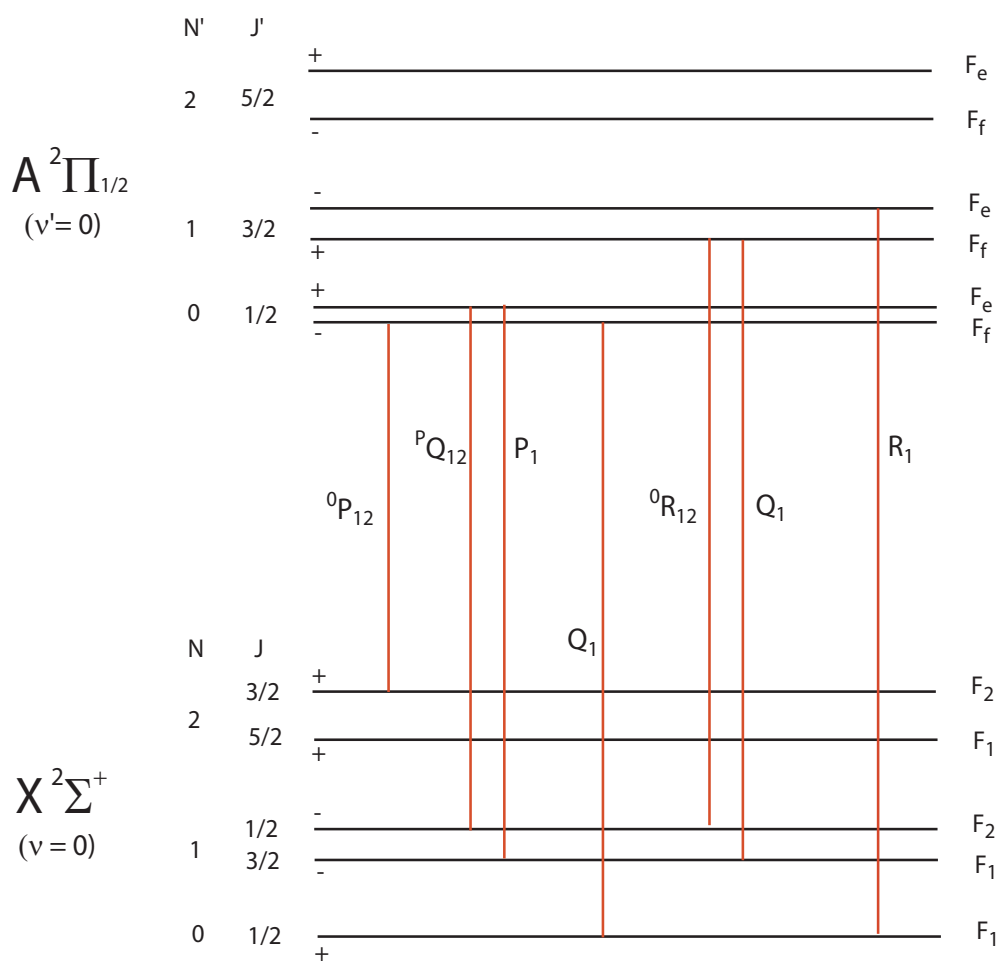


Figure 16: Energy levels of the X and the A states and definitions of branches

a given lower state according as the parity of the lower state is odd or even. The  $\Lambda$ -doubling does not result in additional transitions lines.

In the presented study we always drove the transition for the  $Q_1(0)$  line at a frequency of  $542811 \pm 1$  GHz, when we did not scan the laser frequency but locked it to this frequency to study the YbF production. As we will later see it turned out that is hardly implementable to record a YbF absorption spectrum under those conditions we are faced with in our setup.

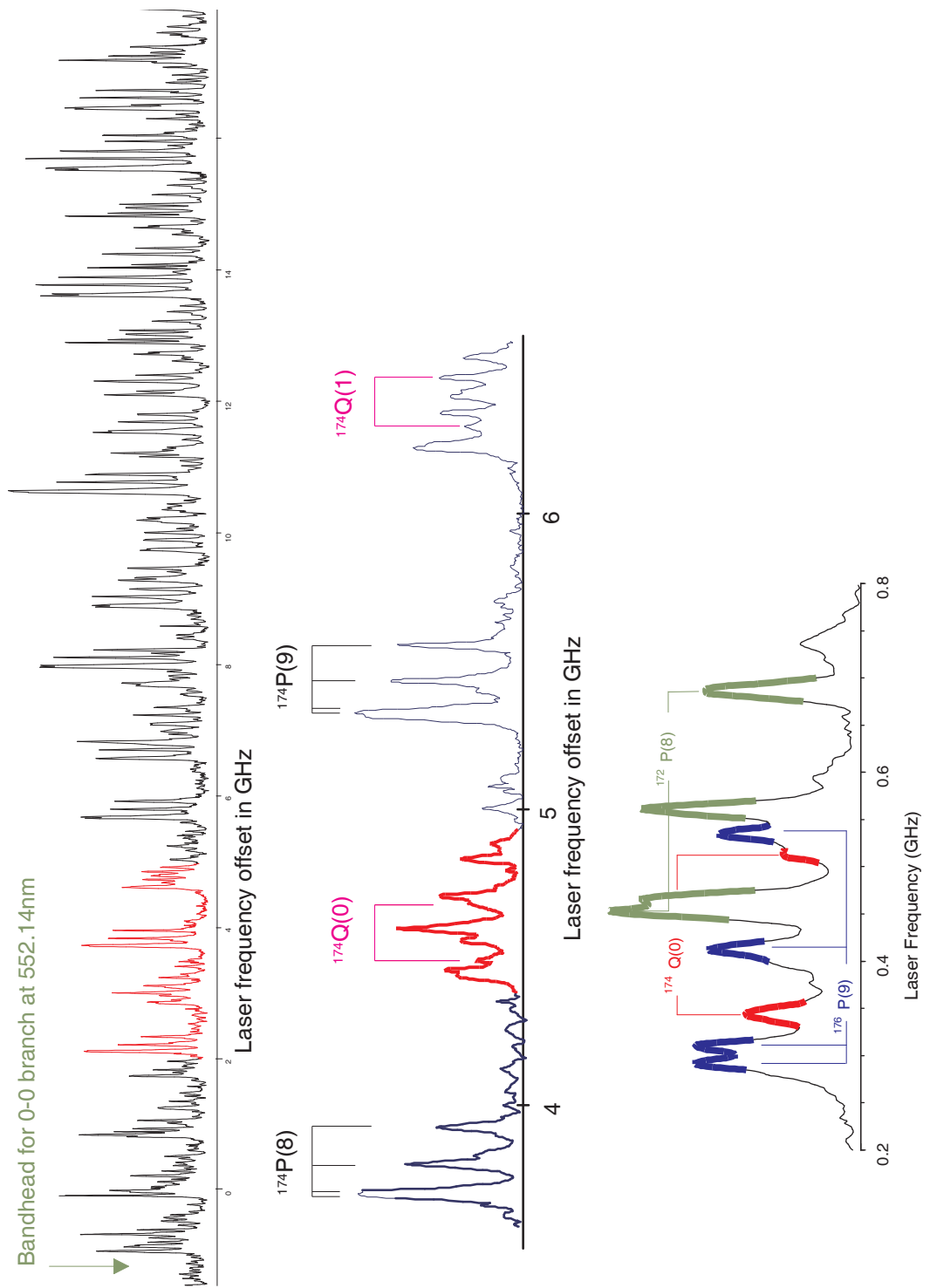
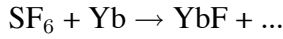


Figure 17: Band head structure of YbF

### 3.3 Mean free path

The formation of YbF in the environment of Ar/SF<sub>6</sub> is based on collisions between the ablated Yb (hot) and the fluorine containing SF<sub>6</sub> as follows:



Additionally to that, we expect higher order Yb-F connections, such as YbF<sub>2</sub> and YbF<sub>3</sub>.

But in order to get a high enough reaction rate for the first reaction, the mean free path for the reactants should be about D/100, where D is the typical distance to the next wall of the ablation cell. For this threshold, the Yb atoms are supposed to have reacted with SF<sub>6</sub> to YbF.

The mean free path  $\lambda$  is given by

$$\lambda = \frac{RT}{\sqrt{2}\pi d^2 N_A p} \quad (15)$$

where d is the molecular or atomic diameter of the reactants. Assuming d to be about 0.2 nm, we get the following mean free path for different temperatures depending on pressure as shown in Figure 18:

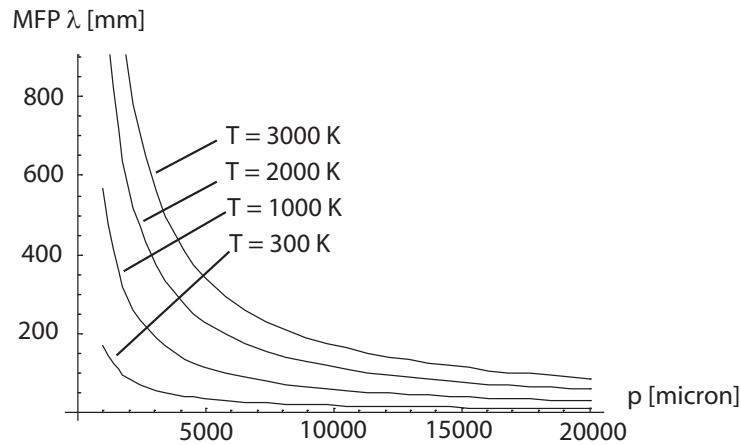


Figure 18: Mean free path for different temperatures

Since the ablated Yb is supposed to be hot, we assume a temperature somewhere in between room temperature (300 K) and 3000 K. Later on we will get

more information about the temperature. But as far as we can see, the buffer pressure inside the cell should be well above 1000 micron in order to get a sufficient number of YbF. Therefore, this might be a good starting point for our pressure study with respect to the number of produced YbF.

## 4 Testing the Setup

At the very early days of this experiment we did a lot of test measurements with the setup in order to get an impression of the ablation processes inside the cell.

### 4.1 Yb absorption signal

One of the first aspects we were looking at was an absorption signal for Yb. The question was whether we were able to see any signal for an ablated material with this setup or new kind of molecule source.

This is a short description of the first test measurement: Yb atoms are ablated by a pulsed YAG laser that is aligned right to the Yb target surface. The ablated Yb can be detected or observed with a probe laser beam passing perpendicular to the incoming YAG light. The probe laser beam is aligned such that it is just tangent to the targets surface, i.e. the distance between target surface and probe beam lies in between 0.5 mm and 1 mm whereas the beams diameter is roughly 1 mm.

For this first measurement we used a different YAG laser than described above, namely that YAG which is used for the current decelerator experiment. This YAG emits 10 ns long laser pulses at  $\lambda = 1064$  nm with a repetition rate of 10 Hz. We run it at 80% of maximum power.

The probe laser was locked to the well known frequency for the  $^1S_0 \rightarrow ^3P_1$  transition for Yb at  $539386 \pm 1$  GHz. The probe beam power amounts to  $1.2 \pm 0.1$  mW before passing the ablation cell.

At that time we did not have to the possibility to measure the inside pressure below atmosphere pressure, but for this first test we pumped the cell down to rough vacuum. So the pressure laid between 100 micron (bottom pressure for vacuum pump) and 1000 micron.

Since there was no data acquisition with a computer available yet, we recorded the absorption signal with an oscilloscope electronically triggered by the YAG pulses.

Fortunately, we could see an absorption signal and its time evolution for the first 0.5 ms on the scope.

## 4.2 YbF absorption signal

With this very early setup we also tried to observe an absorption signal for YbF. Therefore, we filled the ablation chamber with a buffer gas (Ar) containing a small fraction (2%) of SF<sub>6</sub>.

We adopted the settings for the YAG laser and the alignment for both, the YAG and the probe laser, but changed the frequency of the probe laser to the Q(0) line for the  $A^2\Pi_{1/2} - X^2\Sigma^+(\nu = 0)$  of YbF at  $542811 \pm 1\text{GHz}$ .

And also in this case we were lucky enough to observe an absorption signal, presumably YbF.

In order to get a vague overview over the absorption's dependence on pressure we took a couple of absorption profiles for different pressures of Ar/SF<sub>6</sub>, even for pressures above atmosphere. At this stage of the experiment setup we temporarily used a pressure gauge with a quite unusual scale in "inch Hg".

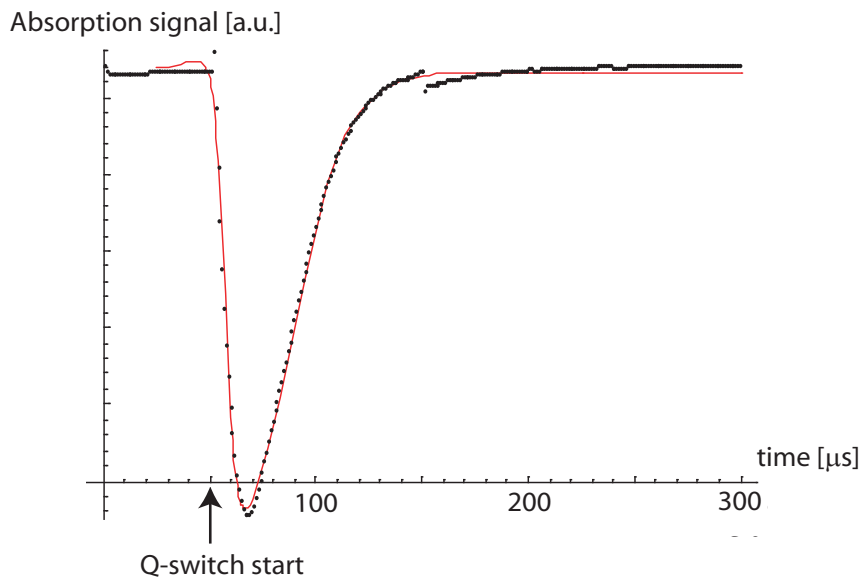


Figure 19: YbF absorption profile

Regarding the absorption profiles of YbF for different pressures we can say - very roughly speaking - that increasing the pressure makes the absorption lines deeper and more intensive. In general we could achieve 50% to 70% of absorption. The drop down seemed to be exponential, so we tried to fit the absorption profile with the following function:

$$F_{fit} = C_{offset} + (C_{max} - C_{offset}) \cdot \left\{ \frac{a_1}{a_1 + e^{\gamma_1(t-t_1)}} + \frac{a_2}{a_1 + e^{-\gamma_2(t-t_2)}} \right\} (16)$$

with  $t$  as the fit variable and whereas all the other variables are fit parameters. Figure 19 shows one of these fits and its astonishing accuracy.

To conclude this section, we are able to produce YbF and to detect it with this apparatus. The setup seems to be sufficient enough to proceed with in order to get more detailed information, such as the production rate of YbF, the optimal buffer gas pressure to operate at and the YbF diffusion inside the ablation chamber.

## 5 Yb Spectrum

Figure 20 shows a picture of the ablation plume as it can be observed through the one of the probe beam windows. This picture was taken without any buffer gas inside the chamber at rough vacuum ( $\sim 0.3$  Torr). The size and the colour of the plume suggest that the jet of ablated Yb is extremely hot and that Doppler-broadening is likely to have a dominant effect on absorption spectroscopy.



Figure 20: Picture of the ablation plume that was taken without any buffer gas inside cell at rough vacuum ( $\sim 0.3$  torr)

### 5.1 Yb absorption spectroscopy

In order to estimate the effect of Doppler broadening and a temperature of the ablated Yb atoms in the plume we did a frequency scan over a well known part

of the Yb spectrum. The following data were already taken with the final setup as described in section 2 apart from the YAG laser ("Quantel brilliant b" instead of "Quantel brilliant") and the gas and vacuum system which were still coupled at this time.

Figure 12 shows the setup for this spectrum scan. Yb atoms are ablated by a pulsed YAG laser ( $\lambda = 1064\text{nm}$ , energy/pulse = 185mJ, flashlamp frequency = 10Hz, pulse duration = 6ns) and detected with a probe laser regarding the absorption signal. The cell was pumped down to rough vacuum at  $\sim 100$  micron.

The part of the Yb spectrum we were looking at includes the hyperfine structure components and isotope shifts of the 555,648 nm line of Yb. So the probe laser was centered to the frequency for the  $^1S_0 \rightarrow ^3P_1$  transition for Yb at  $539386 \pm 1\text{GHz}$ . The scan width was  $\pm 3\text{GHz}$  around this center frequency. Figure 21 shows the measured part of the Yb Spectrum.

## 5.2 Yb spectrum simulation

The plot above also contains a simulation of the expected spectral lines. Since we presume Doppler broadening as the dominant effect on the line width, the simulation is based on a sum of Gaussian functions due to a Doppler broadened line profile. Considering a Maxwell-Boltzmann velocity distribution

$$p(v) \propto v^2 \cdot e^{-\frac{mv^2}{2kT}} \quad (17)$$

we obtain for one dimension, in which we were actually detecting with the probe beam perpendicular to the ablation plume, a 1-dimensional velocity distribution

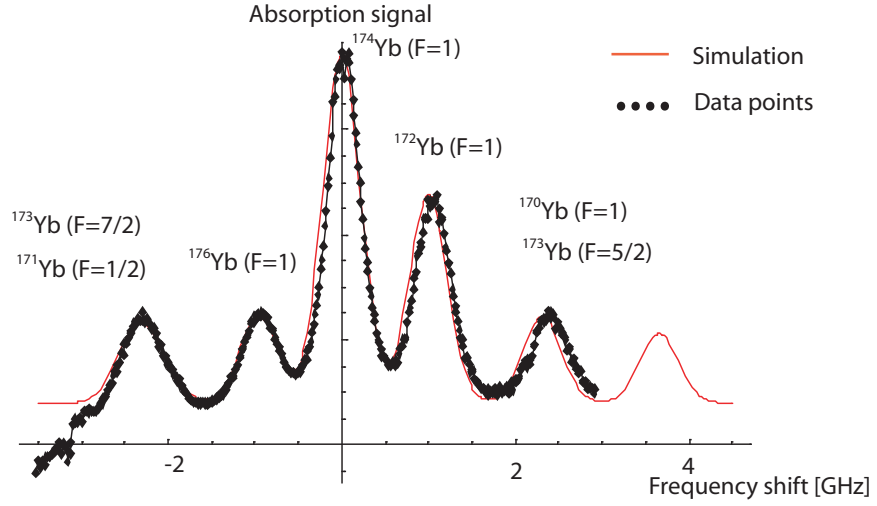
$$p(v_x) \propto e^{-\frac{mv_x^2}{2kT}} \quad (18)$$

The Doppler shift is given by

$$\frac{\Delta\nu}{\nu_0} = \frac{\nu - \nu_0}{\nu_0} = \frac{v_x}{c} \quad (19)$$

If we put equation (19) into equation (18), we get

$$p(\nu_x) \propto e^{-\frac{m}{2kT} \cdot \left(\frac{c}{\nu_0}\right)^2 \cdot (\nu - \nu_0)^2} \quad (20)$$



Measurement of the hyperfine structure components and isotope shifts of the 555,648 nm line of Yb, relative to  $^{174}\text{Yb}$

Figure 21: Measurement of the hyperfine structure components and isotope shifts of the 555,648 nm line of Yb

and with  $c = \lambda_0 \cdot \nu_0$  we obtain a Gaussian profile for the spectral lines dominated by Doppler broadening

$$p(\nu_x) \propto e^{-\frac{(\nu-\nu_0)^2}{w^2}} \quad (21)$$

whereas the line width  $w$  is given by

$$w = \frac{1}{\lambda_0} \sqrt{\frac{2kT}{m}} \propto \sqrt{T} \quad (22)$$

As already mentioned above, the simulation shown in Figure 21 is a sum of Gaussian curves as given by equation (21):

$$Simulation = \sum_i offset_i + amplitude_i \cdot e^{-\frac{(\nu - \nu_0 - b_i)^2}{w_i^2}} \quad (23)$$

whereas  $w_i$  is the according width for each line with respect to the different masses of the Yb isotopes and  $b_i$  is the frequency shift of each line relative to the  $^{174}\text{Yb}$  (F=1) line.

As we can see from Figure 21 the line width is about 1GHz and the simulation reveals a temperature of about 3000K to 5000K for the ablated Yb atoms inside the plume jet shown in Figure 20.

## 6 YbF scan near bandhead

Before we can discuss the formation process of YbF and its dependent parameters, we should search for any evidence that the observed absorption signal we have presented in chapter 4 is really due to YbF. Although we know the frequency of the transition which we would like to detect YbF with, and although we get an absorption resonance for that frequency it is not fairly obvious that it is and only is related to YbF. Therefore, we did a frequency scan with the probe laser near the bandhead of the  $A^2\Pi_{1/2} - X^2\Sigma^+(\nu = 0)$  transition of YbF (see Figure 17).

For this scan we proceeded as we did for the Yb spectrum apart from the fact that we now needed Ar/SF<sub>6</sub> inside the ablation chamber to form YbF (buffer gas pressure 10,000 micron). We scanned the probe beam over a scan width of  $\pm 10$  GHz around a center frequency of  $542805 \pm 1$  GHz, which is 6 GHz below the Q(0) line and very close to the regarded bandhead.

Figure shows what we could observe by using a reference signal in order to compensate the intensity drift discussed in the previous chapter.

The absorption signal clearly shows a sudden jump to a higher level of absorption at a frequency of about  $542806 \pm 1$  GHz. At higher frequencies than this mark there is obviously more absorption observable.

In comparison to the reference spectrum of YbF near the bandhead (see Figure 17) these data suggest that this jump in the absorption signal is due to the bandhead of the  $A^2\Pi_{1/2} - X^2\Sigma^+(\nu = 0)$  transition of YbF for about the same frequency.

One might claim that this evidence to YbF is not sufficient and convincing enough, but so far we are fairly convinced that we detect YbF in the ablation chamber.

Unfortunately, as we have seen in the previous chapter Doppler broadening is the dominant effect in any spectra taken under these extreme ablation circumstances. Therefore, the lines in the YbF spectrum are broadened to a width of 1 GHz so it would be hardly possible to observe a clear YbF spectrum that could provide an unimpeachable evidence to YbF. In fact, we tried to observe a YbF spectrum, but the data are not conclusive. Even the trial to prove the band structure of the YbF spectrum instead of observing particular lines does not give more information, i.e. although each band covers a frequency range of some ten GHz and they are separated by gaps of about the same size, we could not manage to observe a signal where we can clearly see parts of high absorption due to bands separated by parts with low absorption due to the gaps. We always got some ab-

sorption signals in the gaps where they are not supposed to appear.

Nevertheless, we are going to proceed the study since we believe that we detect YbF. A Doppler free spectroscopy could give more evidence. That could be implemented by letting the YbF expand through a hole in the chamber and then applying the Doppler free spectroscopy.

## 7 Target Lifetime

As already mentioned above, the current source for YbF molecules used in the decelerator and the EDM experiment is faced with some problems due to the target lifetime, i.e. the flux of molecules decays as the target ages. This study aims to understand the ageing process of the target and perhaps to find better conditions so that the target lasts for a longer time and provides a nearly constant flux of YbF molecules over a longer time scale.

### 7.1 Current source

In order to give a briefing about the current technology we would like to present some characteristics about the target lifetime of the current molecule source and its determining parameters:

- If the ablation laser strikes the same place on the Yb target many times, the detected YbF signal deteriorates exponentially. With a  $\sim 2$  mm spot the target in the current source lasts for about 5000 shots of the pulsed YAG, i.e. in units of time this decay time corresponds to 500 sec. with a 10Hz pulse rate.
- After that time the source does not provide a sufficient flux of molecular radicals and the target wheel has to be turned a little bit so that the YAG hits the Yb target at a different spot (see Figure ).
- We presume that this decay is probably caused by drilling a hole in the target, although it may also be related to a blackened layer that builds up on the surface of the target.

### 7.2 Target Lifetime Study

One aspect of the present study addresses the aspect of target lifetime with respect to the energy in the ablation pulse and the pressure of buffer gas inside the ablation cell.

Thus, we tried to see whether we are faced with the same problems summarized above while forming YbF by laser ablation with this setup.

We did a sequence of experiments where we shot the YAG onto the Yb target and observed what happened to the absorption signal and other parameters that give information about the target lifetime such as the size of the ablation plume and the shape the YAG spot at the target surface. The time-averaged YAG power was about 1.1 W. The typical probe beam power lay in between 1 mW to 2 mW with a beam diameter of 1 mm.

What we observed was quite similar to what had already been recognized for the current source: If the YAG laser strikes the same place on the target many times, the YbF signal - in this case the absorption signal of the probe beam - deteriorates in time. The size of ablation plume also decreases with an increasing number of YAG shots on the same spot. Starting with a cleaned and filed surface, the ablation plume is about 1 cm to 2 cm long (buffer gas pressure  $\sim 2$  Torr) and then decreases until it is nearly vanished and can not be seen any longer through the windows of the 6-way-cross. We are going to discuss the relevant time scales later on. What we could also observe is a black or grey layer on the target surface.

To conclude, we could repeat similar observations with this apparatus as with the current supersonic source, i.e. a deteriorating YbF signal and a blackish grey layer on the target surface that might cause the decay in the YbF signal.

We assume that the black layer that builds up on the surface of the Yb target might be due to the SF<sub>6</sub> in the buffer gas in that way that maybe a fluorine containing chemical connection overlays on the surface and thus poisons the target.

### **7.2.1 Lifetime Study without buffer gas**

As a consequence of the observations and assumptions above it seemed quite reasonable to study whether we could observe this blackish grey layer even without SF<sub>6</sub> in the buffer. Therefore, we fired the YAG onto the target for about 500 shots at rough vacuum and with pure Ar inside the ablation cell ( $\sim 200$  Torr) and then had a look on the target afterwards. The lasers' powers correspond to those in the previous paragraph.

Contrary to our presumption we could also observe a - in that case - black layer on the surface, both at rough vacuum and with pure Ar inside the chamber. Since Ar is inert it is unlikely to cause these problems, but pump oil from the mechanical vacuum pump could be responsible for that black substrate on the target when the target becomes heated up by the YAG pulses and carbonized pump oil builds up on the Yb surface.

Since the whole apparatus, especially the ablation chamber, had not been cleaned but pumped down quite often for the last two month it is likely that pump oil had propagated through the vacuum pipe and reached the 6-way-cross.

For that reason we cleaned those parts of the setup being in contact with "vacuum". The cleaning procedure for the experiment's components started with an ultrasonic bath in a solvent of detergent (Decon 90) for 30 min. After that, everything was rinsed with tap water and finally cleaned with iso-propanol in the ultrasonic bath, again for 30 min.

In order to avoid pump oil inside the ablation chamber for succeeding experiments, we tried a couple of filter or trap systems for pump oil. It turned out that a combination of an oil absorbing filter and a cold trap consisting of a coil surrounded by liquid nitrogen prevents the oil back-streaming of hydrocarbons from the roughing pump most efficiently. Both systems are described in chapter 2.

When we repeated the previous measurement at rough vacuum with this pump oil filter and trap system there was still a little trace of black stuff at the edges of the spot where the YAG stroke the target, but compared to the situation before having cleaned the cell and using the filter-trap system the target is much less affected by the black layer. So, we can assume that pump oil really caused the layer during the lifetime study without buffer gas and is now minimized to a certain level by the trap system for pump oil.

For a succeeding implementation of a buffer gas cooled source for cold molecular radicals using laser ablation we suggest a different type of vacuum pump, e.g. a turbo pump, where the effect of pump oil does not appear.

The next stage in the study of target lifetime focuses on the energy in the ablation pulse. In former studies one found a threshold intensity per pulse of  $10^7$  W/cm<sup>2</sup> for vaporizing the Yb target. Therefore our study concentrates on intensities above this value. We ablated Yb atoms for different YAG intensities and looked at the effect on the target itself, i.e. the physical effects on the surface, but also at the size and form of the ablation plume and the absorption signal for the ablated Yb. We varied the YAG power between 0.75 W and 2.4 W. These are time averaged values, i.e. with a repetition rate of 20 Hz for the Quantel Brilliant YAG laser 2.4W corresponds to an energy of 120 mJ per pulse. The YAG spot typically has a diameter of  $\sim 2$  mm.

The following conclusion were drawn from this investigation:

- It turned out that the lowest energies (0.75 W) are not effective enough to ablate a sufficient number of Yb, so we could not even observe a visible ab-

lation plume. In that case the target surface only turns dark due to thermal effects of the YAG.

- The higher the ablation energy gets the more intensive the plume grows and the stronger the effect on the surface becomes.
- For the highest energies regarded, i.e. 2.4 W, the YAG drills a deep hole in the target and even reaches the opposite side. In that case the drilling effect causes the signal decay.
- The absorption signal for Yb decays with an increasing number of shots, but does not become smaller than 75% of its starting value after 10,000 shots. And even after 15,000 shots the target provides the 50% of the absorption signal.
- The size of the ablation plume also decreases in time. That might be on the one hand due to the YAG drilling a hole into the target, so that less Yb is ablated, and on the other hand due to the fact that the increasing number of Yb inside the cell reduces the mean free path for the Yb atoms and therefore reduces the size of the ablation plume.
- We always could observe two dips in the time evolution of the absorption signal. In that case, where we just ablate Yb into rough vacuum, we guess that the second dip is due to Yb atoms bouncing back from the walls of the ablation chamber and then re-entering the detecting zone of the probe beam.

The following estimation shall corroborate this presumption. Assuming a temperature of about 3,000 K for the ablation plume the velocity for the Yb ( $m = 174 \text{ g/Mol}$ ) atoms is given by

$$v = \sqrt{\frac{2kT}{m}} \simeq 500 \text{ m/s} \quad (24)$$

The average temporal distance between the two dips in the time evolution of the absorption signal can be estimated by  $t = 200 \mu\text{s}$ , whereas the typical distance to the walls is  $\sim 5 \text{ cm}$ , so the total flight distance for the forward and backward movement of the atoms bouncing back from the walls is  $s = 10 \text{ cm}$ . In that case we have a velocity of

$$v = \frac{s}{t} \simeq 500 \text{ m/s} \quad (25)$$

which is in good agreement with our presumption.

Considering these aspects we finally decided to proceed with a YAG power of about 1.2 W (time average) according to a flashlamp/Q-switch delay time of 330  $\mu\text{s}$  since on the one side this energy level per pulse provides a stable Yb signal for at least 15,000 shots, but on the other side does not damage the target to the same extent as we could observe for e.g. 2.4 W.

However, later on we had to diminish the power to 0.75W according to a flashlamp/Q-switch delay time of 350  $\mu\text{s}$  since we used a focussing lens to reduce the size of the YAG spot (diameter  $\sim 1.5$  mm) but wanted to keep the power per unit area constant. All data presented later on were taken with this YAG power of 0.75W

### 7.2.2 Lifetime Study with buffer gas

Since we had not answered the question yet whether the  $\text{SF}_6$  has any effect on the target lifetime, we studied the target lifetime for different buffer gas pressures ( $\text{Ar}/\text{SF}_6$ ). We focussed our interests on the absorption signal for YbF formed by laser ablation, when the YAG strikes the same spot many times, the effect on the target itself, i.e. the physical effects on the surface, but also on the size and form of the ablation plume. For a particular pressure we took data of the time evolution of the YbF absorption signal after each shot and averaged over a block of 500 shots and proceeded until the absorption signal was too small to detect.

Figures 22 and 23 show the maximum of the averaged absorption signal (maximum means maximum in the time evolution of the absorption signal, typical time scale 2ms) versus the number of YAG shots for particular buffer gas pressures. These two pictures are examples chosen to demonstrate how the absorption signal deteriorates in time for different pressures.

The following conclusions were drawn from this investigation:

- The target lifetime in the sense of the magnitude of the absorption signal for YbF deteriorates in time.
- The target lifetime varies between 7,000 shots and 30,000 shots depending on the buffer pressure inside the cell
- In general we can say that the higher the buffer gas pressure the shorter the target lifetime.
- There are mainly two reasons for the different target lifetimes:
  - The YAG terminates the target lifetime by drilling a hole in the target. This is clear since it means that less ablated Yb collides with the  $\text{SF}_6$

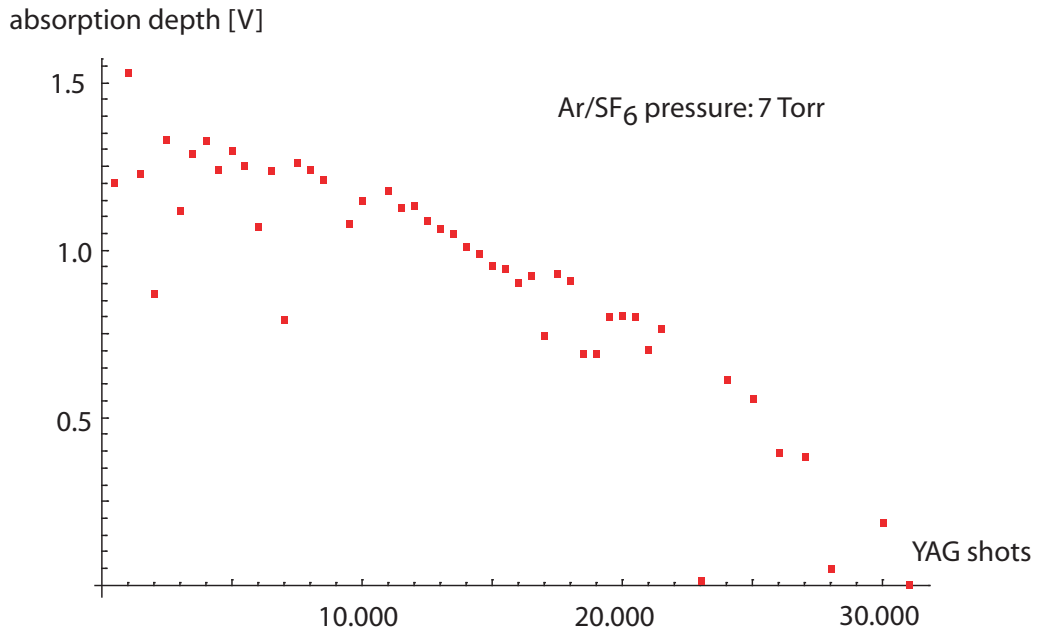


Figure 22: Target lifetime for buffer gas pressure 7,000 micron. The plot shows the decay of the absorption signal for YbF versus the number of YAG shots

and therefore the production rate of YbF decreases. This phenomenon mainly occurs for lower pressures, i.e. between 1,000 micron, where we started our investigation and 15,000 micron.

- We could observe a blackish grey layer on the target surface where the YAG hits the target. The grey area has a similar form and size to the YAG spot itself. This layer usually builds up for pressures higher than 15,00 micron. It seems that this grey substrate is similar to Yb-ash flakes which appear while producing YbF setting down on the walls of the ablation chamber. This grey substrate might prevent the ablation of Yb below this layer, and it has to be clearly distinguished from the black layer we were faced with while ablating Yb in rough vacuum without a buffer.

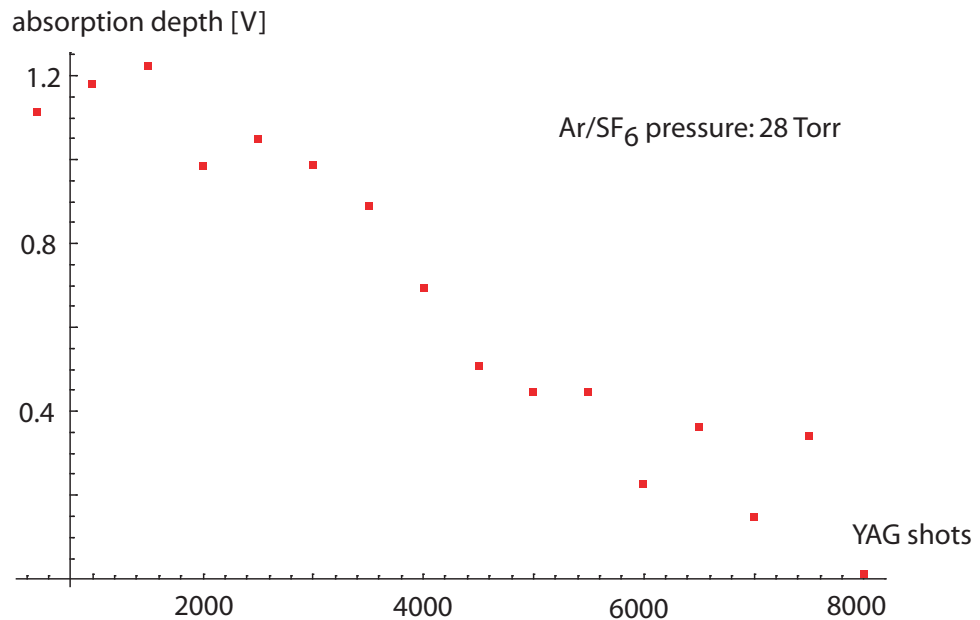


Figure 23: Target lifetime for buffer gas pressure 28,000 micron. The plot shows the decay of the absorption signal for YbF versus the number of YAG shots

A trial to blast this layer away from the target surface by increasing the YAG power partly worked, but we were never able to return to the former full absorption signal, when the surface was still clean. But we did not follow up this approach of extending the target life.

To conclude this chapter about the target lifetime, we would like to summarize the important facts:

- In comparison to the current technology of the molecule source for the decelerator experiment, this approach of a new source has a longer target lifetime, i.e. the logarithm of the absorption signal, which we assume to be proportional to the number of produced YbF molecules, stays acceptable for at least 10,000 shots compared to 5,000 shots for the current source.

- The target lifetime depends on the buffer gas pressure and - roughly speaking - the target lifetime decreases with increasing pressure.
- A trial to re-clean the target by blasting the poisoning layer away does not seem to be promising
- However, no target or source lasts for ever and so the target lifetime is finite anyway. The target wheel used in the current molecule source is supposed to be a sufficient solution in order to compensate the finite target lifetime. In that case a wheel loaded with Yb samples can be easily turned to another spot after the YAG has hit the target on the same place for many times and this spot does not provide a sufficient number of molecules any longer (see Figure 1).

## 8 Dependence of YbF Production on Buffer Gas Pressure

One important point of this study addresses the production rate of YbF molecules, since the approach with this new kind of source for molecular radicals is supposed to provide a higher number of molecules than the current one.

Therefore, we studied the production rate of YbF with respect to the buffer gas pressure, a parameter we can easily control. The modification of the gas and vacuum system described in section 2, where we have separated the vacuum output from the buffer gas input, allows us to keep a constant flux of "fresh" buffer gas through the reaction zone and thus to keep the pressure inside the ablation cell stable as we are producing YbF.

A first study delves into the dependence of the time evolution of the absorption signal on different buffer gas pressures. Figure 24 shows the absorption profiles of YbF for different pressures. Each profile is an average data set over 200 profiles according to 200 shots of the ablation laser. The single profiles did not deviate very much from the average profile, so we can assume that the absorption signal is quite stable for the first few hundred shots.

In that case the horizontal distance between the target surface and the probe beam amounted  $\sim 2$  mm, whereas the YAG spot and the probe beam were at the same vertical position.

Figure 25 shows a cross section through Figure 24 at the position of the maximal absorption peak. For the lower pressures the absorption peak seems to increase linearly with rising pressure, but at about 14,000 micron the signal promptly drops down and slightly recovers for higher pressure values. This indent can also be observed in the integrated signal, i.e. if we regard the integral over each absorption profile versus pressure (see Figure 26), and if we plot the logarithm of the absorption depth versus the Ar/SF<sub>6</sub> pressure.

The linear part in Figure 24 seems to be quite reasonable since we expect a higher number of YbF molecules within a higher background of buffer gas, i.e. the possibility for the formation of YbF via collisions between Yb and SF<sub>6</sub> is enhanced with a higher density of SF<sub>6</sub> and thus, a shorter mean free path for the Yb. But that indent still remains quite unexpected and not well understood. We had the idea of a shock wave in the cell, but at this point we cannot find any evidence for this guess. If we regard the integrated signal versus time it seems that the course of the plot behaves like an exponential extenuated increase reaching a saturation plateau for very high pressures, but which is interrupted by this indent at about 15,000 micron. The presumption might be verified by a quite similar study we did for high pressures, but where we are not sure about the correctness

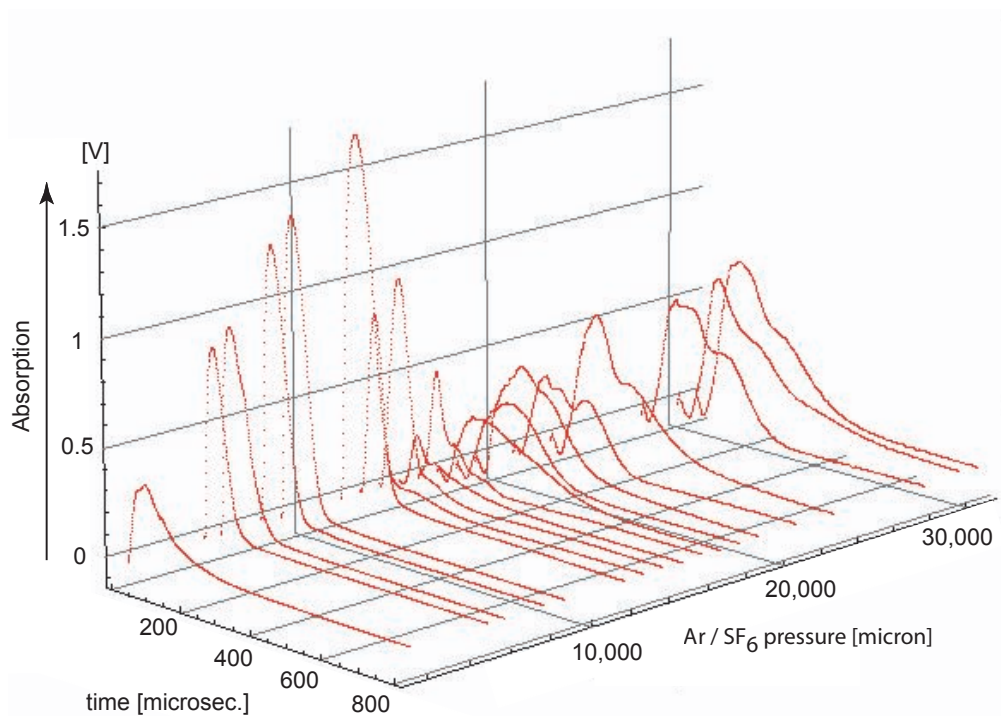


Figure 24: Absorption profiles for different buffer gas pressures. An absorption signal of 2 V means full absorption of the probe beam.

of the data, because the pressure gauge did not provide reasonable values.

N.B.: Regarding Figure 24 we can apparently observe more than one peak in the time evolution of the absorption signal for higher pressures. This phenomenon occurs at pressures of 20,000 micron and above. It seems like that YbF molecules re-enter the detection zone of the probe beam, but not because they bounced back from the walls as was the case with the Yb atoms in rough vacuum but it is rather the picture of molecules colliding with each other and the buffer gas (Ar/SF<sub>6</sub>). So, this might explain why further absorption peaks for later times appear with increasing gas pressure. This collision picture is also substantiated by the fact that the multi peak structure in the absorption signal oscillates in time, which - of course - cannot be seen in the average data in Figure 24.

We repeated these measurements a few times (varying the order in which we took the data for different pressures) and could always confirm what can be seen

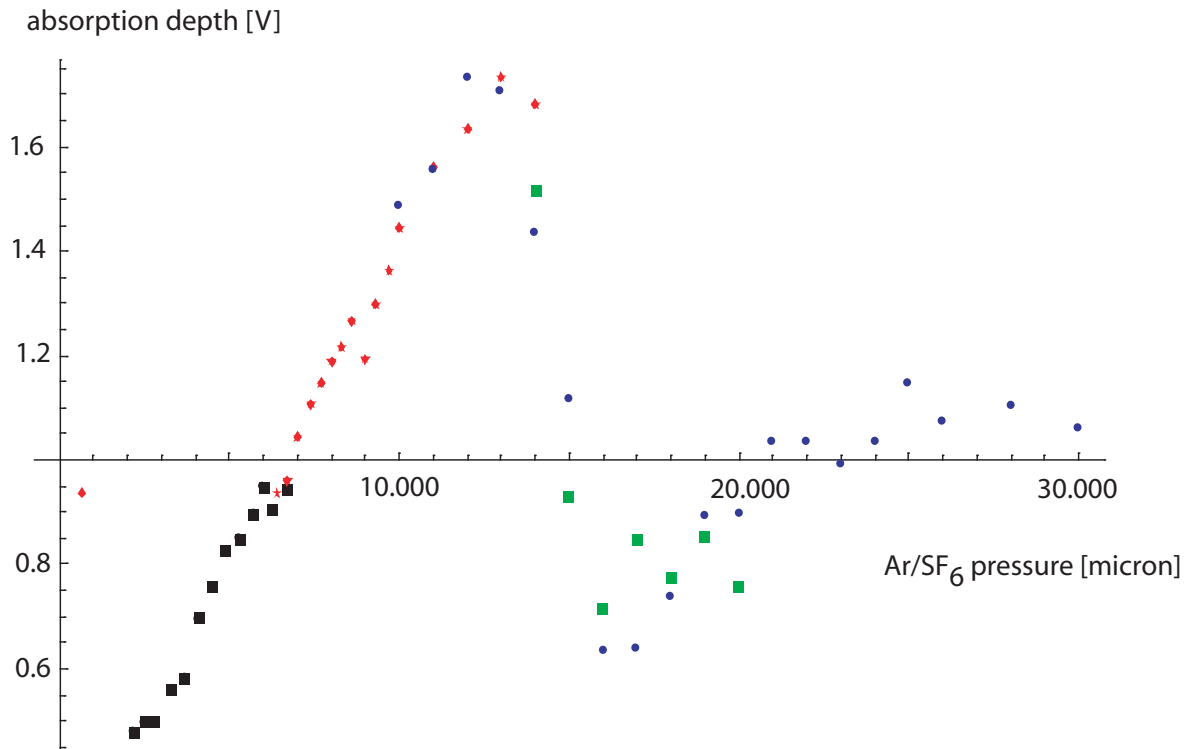


Figure 25: Cross-section through maxima of Figure 24

in Figure 25. The position of the indent in these plots slightly varies with the position of the probe beam, i.e. its distance to the Yb target.

However, the explanations so far are not satisfying and need further investigation. The following section dealing with the diffusion process of the YbF addresses these open questions.

Figure 26 shows the integrated absorption signal for very high pressures. Here we can see that the absorption increases with rising pressure and then reaches a plateau where it saturates. Since the used Pirani vacuum pressure gauge is not really suitable for pressure above 100 Torr, we like to emphasize that the data for pressures below this threshold might be unreliable and considered with caution. For that high pressures the gauge tends to display wrong numbers. But nevertheless, we believe that the formation of YbF must reach saturation since the number

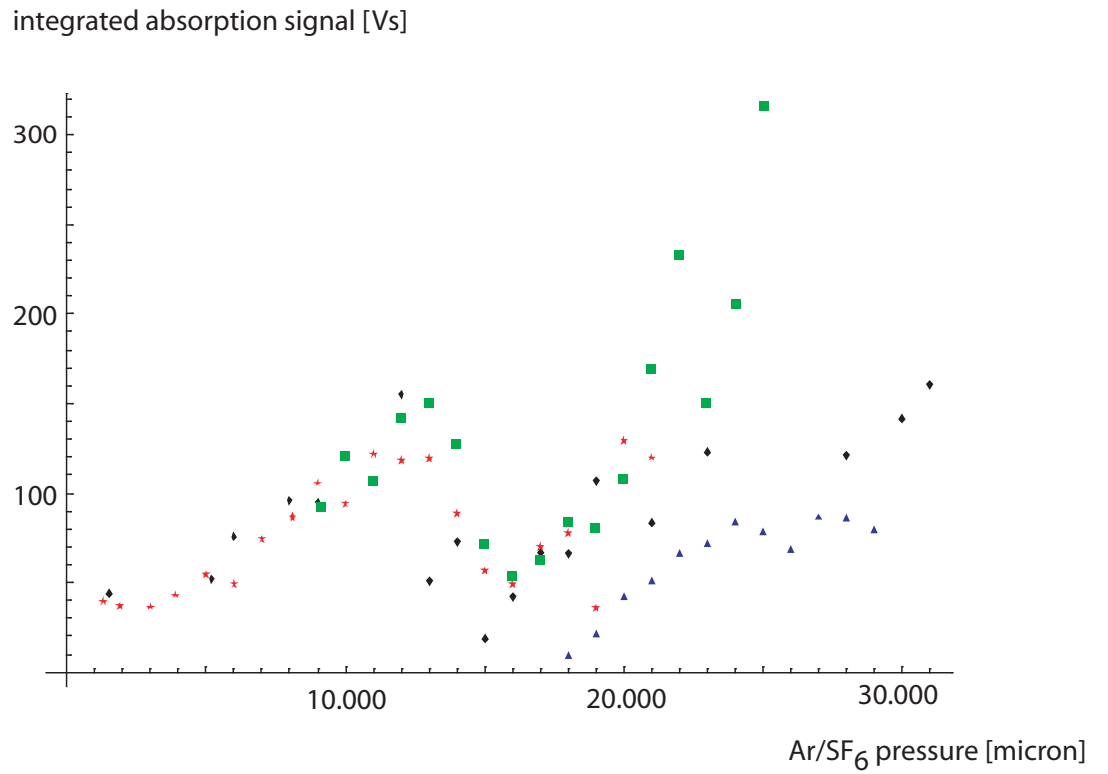


Figure 26: Integrated absorption signals versus pressure

of ablated Yb is finite. But to stress is once more we cannot say for sure that this saturation is already reached for pressures as shown in Figure 26.

## 9 Diffusion and Transport Processes of YbF

As we have seen in the previous section the time evolution of the absorption signals reveals some interesting features such as the indent in the absorption signal depending on the buffer gas pressure that needs further investigation. Therefore, a study of the diffusion behavior of YbF within the buffer may provide a promising view in the ablation and molecule formation process inside the chamber.

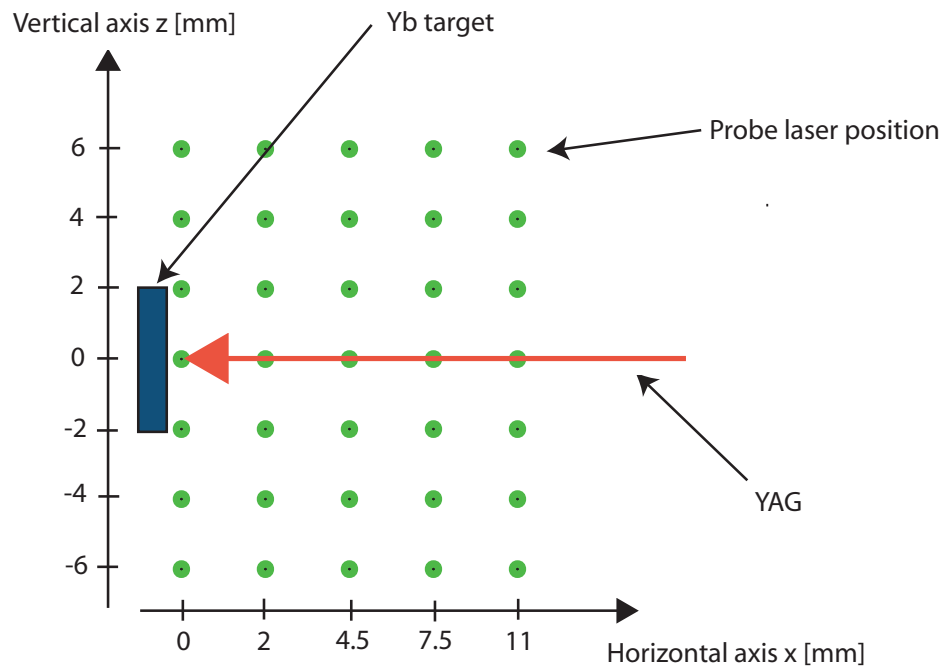


Figure 27: Grid of probe beam positions for YbF diffusion study. The probe beam comes out of the plane perpendicular to the incoming YAG light and has a typical diameter of  $\sim 2$  mm.

For this diffusion study we took an average absorption profile over 100 YAG shots for each point of the grid shown in Figure 27. These profiles - just like those in Figure 24 - give us the time evolution of the absorption signal of YbF, and thus of the density of YbF, at each point of the grid. The time scale typically lies within 0.3 ms and 10 ms. We did this study for different buffer gas pressures while we were able to keep the pressure constant within some few hundred mtorr

for each pressure value ( $\Delta p = \pm 200$  micron).

In the experiment we actually implemented the grid not only by changing the probe beam. Since only the relative distances between the target and the probe beam are important, we controlled the horizontal distances by moving the target rod backwards and forwards via the "Quick connector" (See Figure 5). The vertical distances were regulated by changing the horizontal position of the probe beam with the mirrors M1 and M2 and the fiber output device (see Figure 12) in that manner, that the beam always passed the cell parallel to the optical table, i.e. horizontally.

## 9.1 Two-dimensional diffusion study

The following figures present a choice of snap-shots showing the distribution of the absorption signal over the grid shown in Figure 27. Since we just took data for single points (grid structure) this surface plot was numerically created by interpolation using the single points as mathematical grid points for the interpolation. The sequence of plots for a particular pressure value should give an impression of the time evolution of the signal. However, we recommend to have a look at the Mathematica notebook "Diffusion Study.nb" containing slow-motion movies of these sequences for different buffer pressures. Those movies give a more realistic and instructive impression of the diffusion processes inside the ablation chamber.

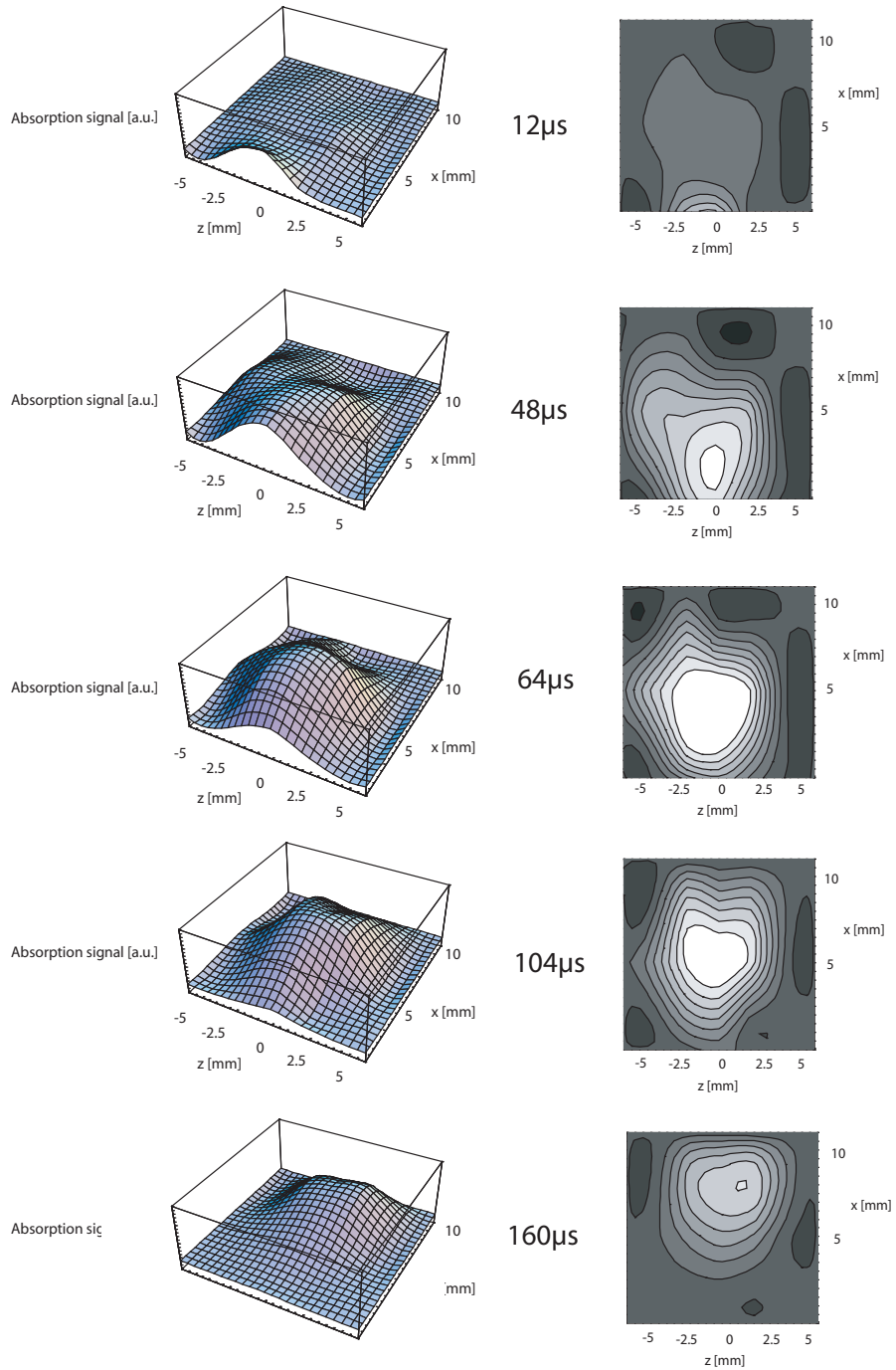


Figure 28: Diffusion process at 7.2 torr

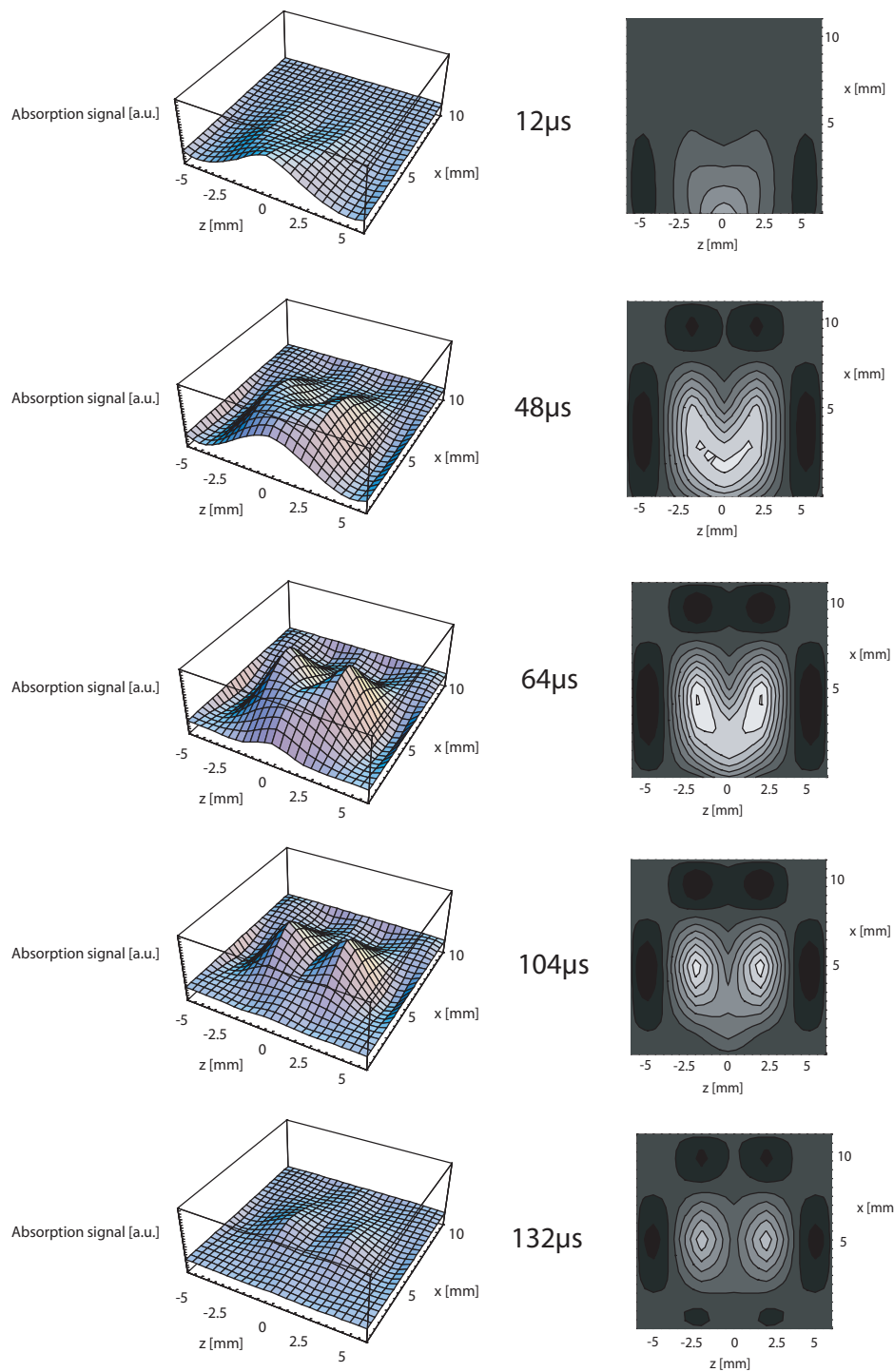


Figure 29: Diffusion process at 12 torr

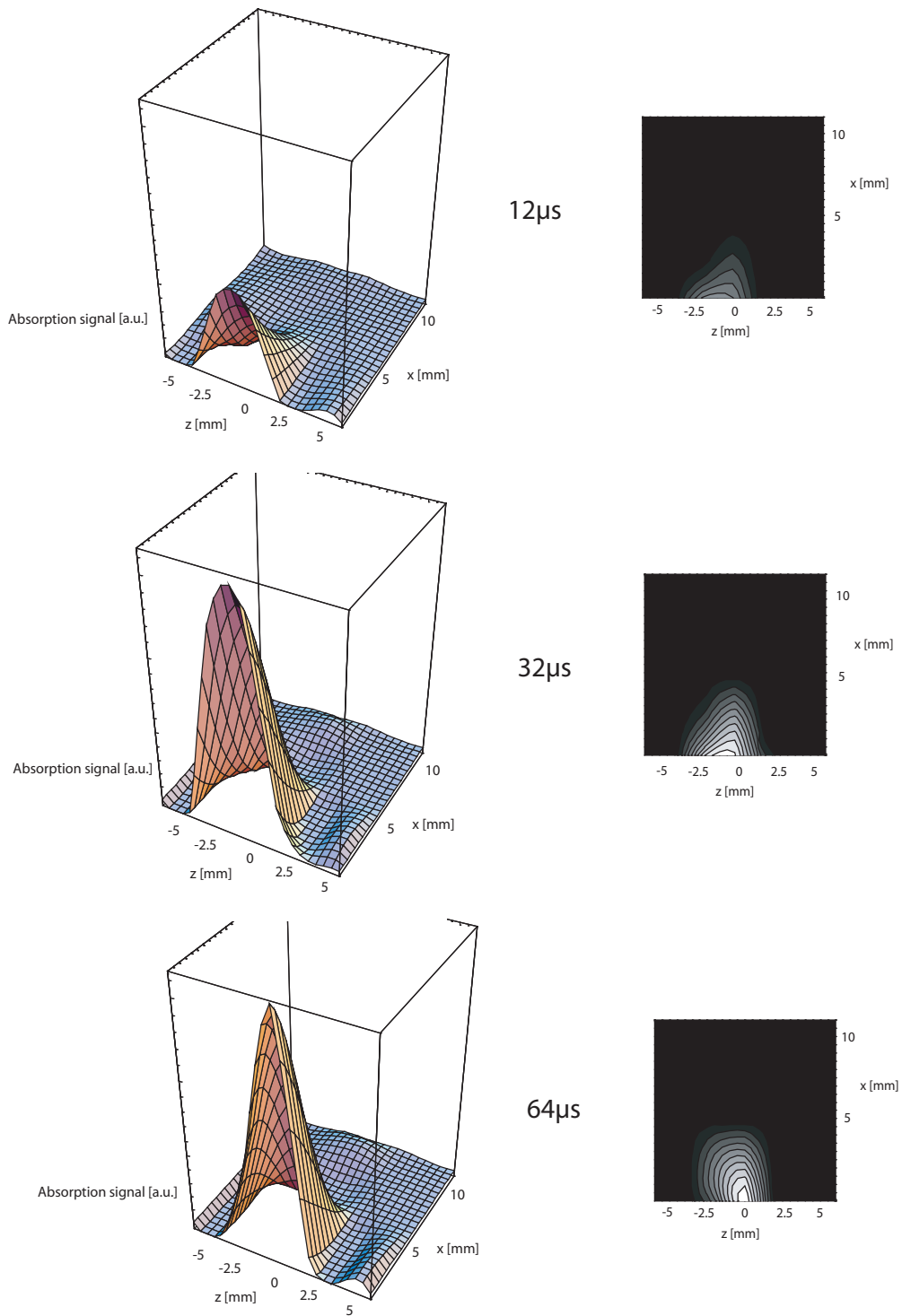


Figure 30: Diffusion process at 14 torr

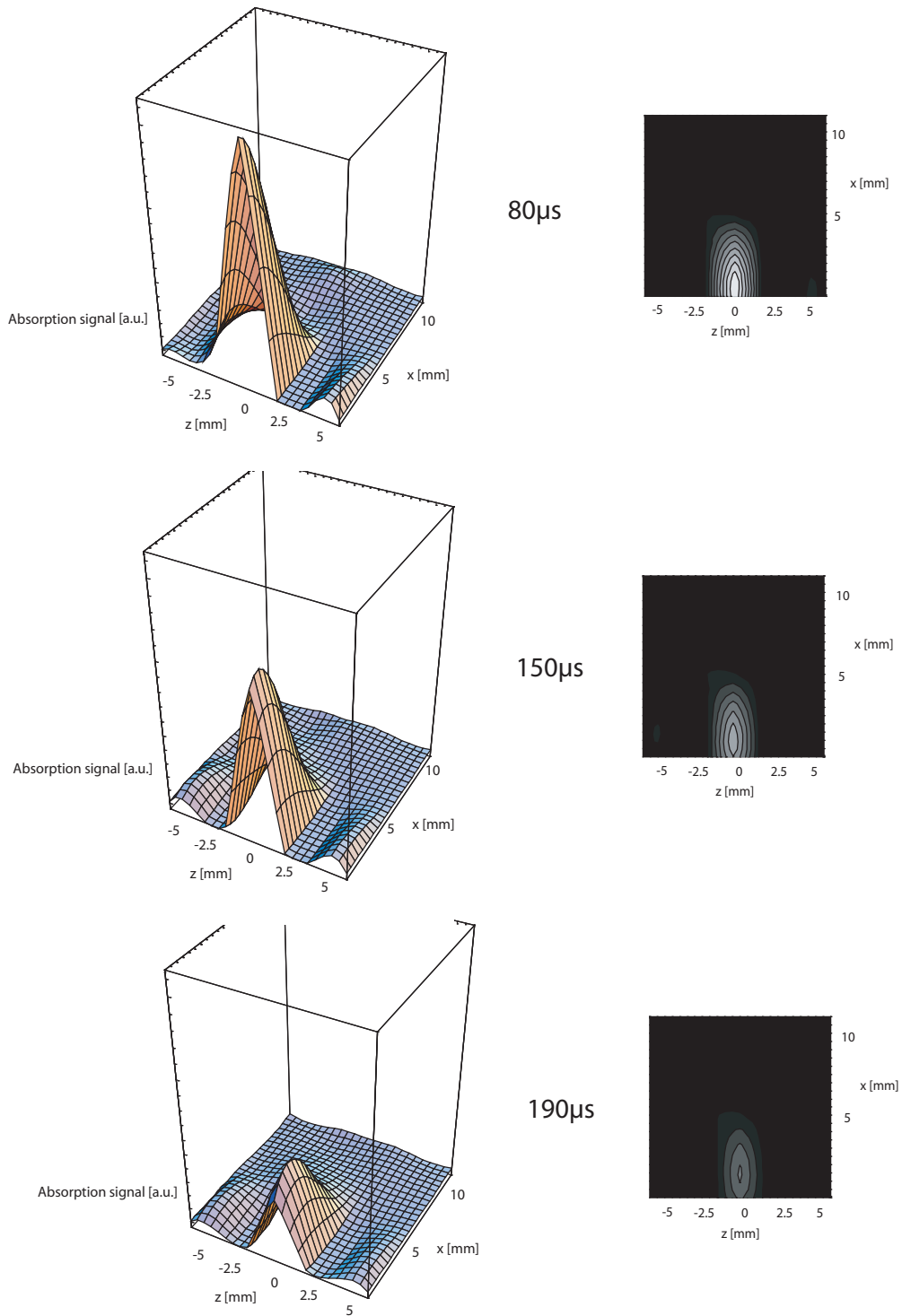


Figure 31: Diffusion process at 14 torr

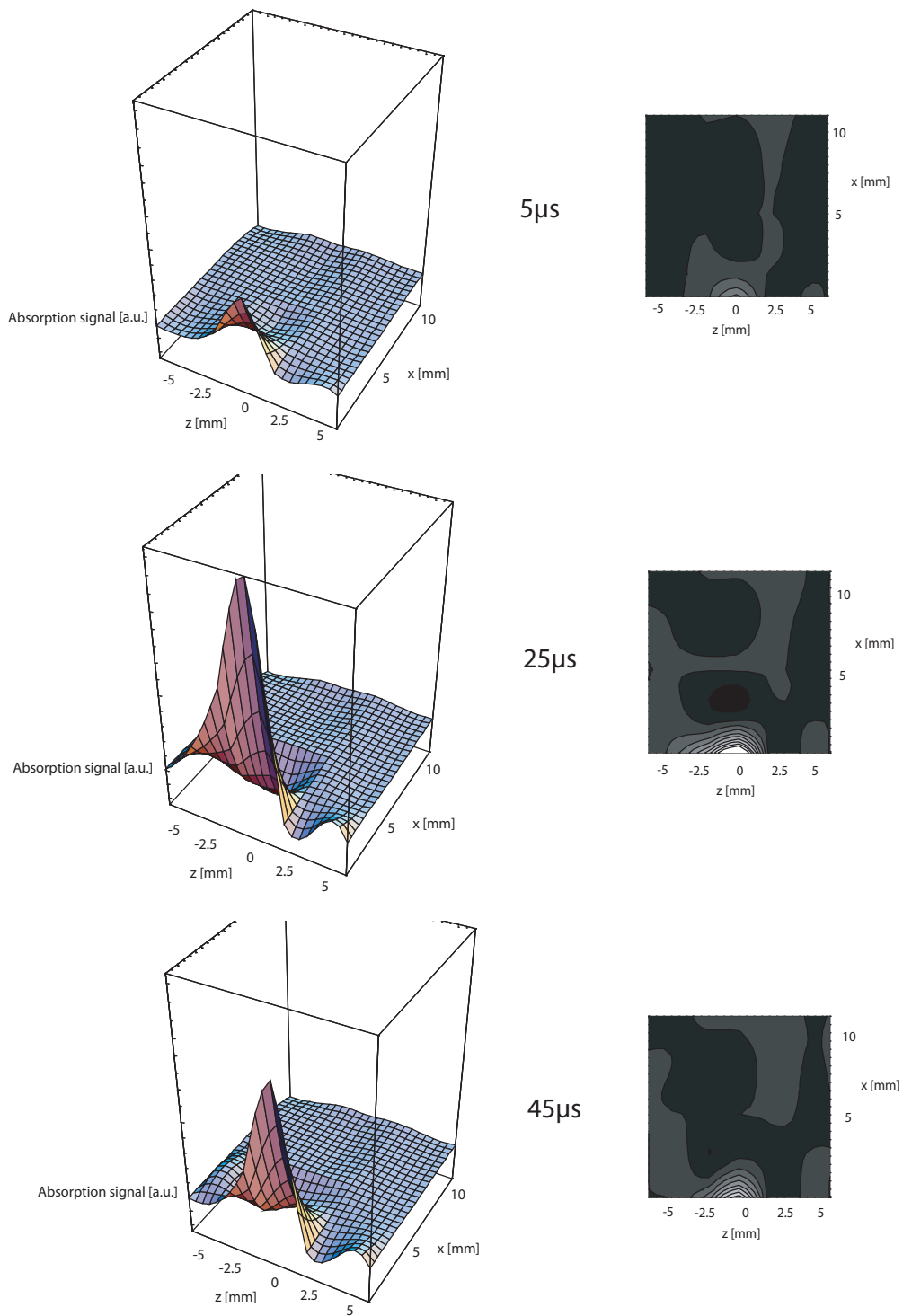


Figure 32: Diffusion process at 17 torr

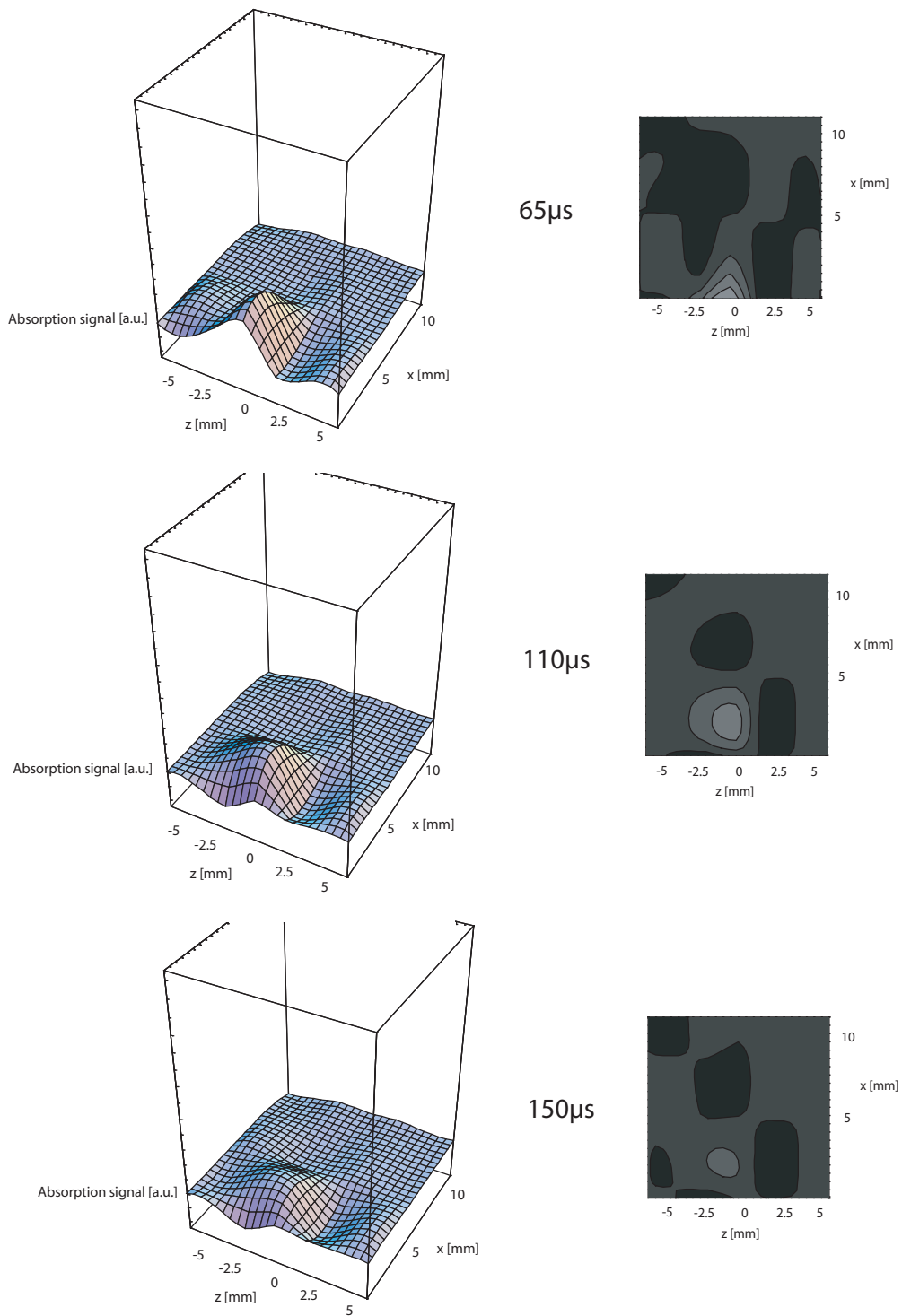


Figure 33: Diffusion process at 17 torr

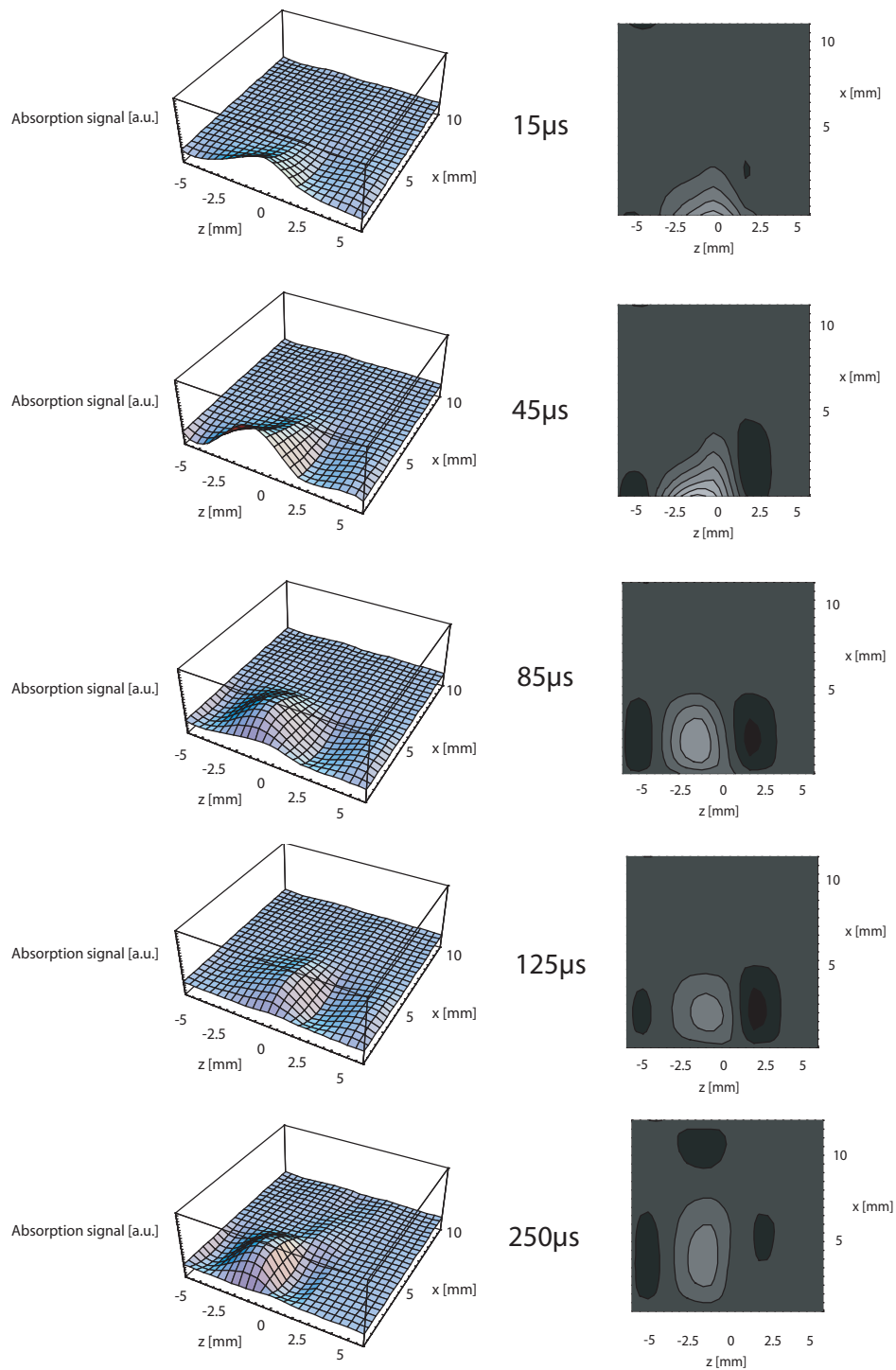


Figure 34: Diffusion process at 25 torr

The following conclusions can be drawn from the figures above:

- Since the YAG light transfers a huge amount of power, more than  $10^7$  W/cm<sup>2</sup>, to the target the Yb gets vaporized and emerges from the surface. As the plume shown in Figure 20 reveals the Yb propagates into a strong forward direction, towards the YAG window. And this forward propagation concerning the bunch of ablated Yb atoms is maintained even after multiple collision with the buffer gas, in which YbF is formed. For that reason we expected the same forward propagation for the formed YbF molecules, but slower than in the case of Yb in rough vacuum due to the shorter mean free path.
- The ablation process itself should not have any priority direction in the y-z-plane, i.e. it should be radially symmetric around the x-axis (incoming YAG beam). Therefore we assume a radial symmetry for the absorption signal and thus for the density of formed YbF. However, the pictures do not present a perfect symmetry with reference to the x-axis, but the signal tends to negative z-values during its time evolution. In the image of propagating molecules that means that the cloud of YbF slightly sinks down to the bottom of the 6-way-cross on its way towards the YAG window opposite the target. Gravity can be excluded since this effect can only be seen on a quite longer time scale. But the ablation apparatus itself induces an asymmetry because we keep a constant flux of Ar/SF<sub>6</sub> passing the cell from top to bottom, i.e. from positive to negative z-values, and this flux of buffer gas could cause the absorptions signal's drift to negative z-values, when down streaming buffer gas transfer momentum in -z direction to the YbF molecules via collisions. This theory is confirmed by the fact that the drift becomes more obvious for higher pressures because in that case we had to work at a higher flux to keep the pressure stable.
- The diffusion study for 7.2 torr shows that for this pressure the diffusion picture approaches what we would have expected. We can see the absorption signal propagating through the cell, or better to say, that is what the pictures suggest. Assuming a certain correlation between the absorption signal and the density of YbF molecules we see a bunch of molecules expanding from the target surface and travelling through the cell counter-propagating the incoming YAG light. The imaged cloud of molecules only slightly changes its shape and dimensions. The highest density of molecule occurs for  $z = 0$  and decreases for increasing  $|z|$ . Figure 35 shows the position of the cross-sections' maximum versus expansion time. As we can determine from the gradient the average expansion velocity is about 500 m/s to 600 m/s. Although we only detected up to 11 mm away from the

target surface the bunch of YbF is believed to travel on towards the YAG window slowly getting less intensive.

- The diffusion plot for 12 torr resembles that for 7.2 torr apart from one fact. In the case for 7.2 torr the bunch of molecules sticks together whereas for 12 torr the bunch splits up into two parts as we can see in Figure 29. Assuming rotational symmetry around the x-axis that means in a three-dimensional space picture that there is a radially symmetric space volume around the x-axis where we detect less YbF than for higher  $|z|$ . We double-checked the obvious symmetry in these pictures to exclude a shifting of our grid, but we verified what can be seen above. For 12 torr the signal does not seem to continue for longer distances rather than collapsing after 300  $\mu\text{s}$  at about 8 mm from the target surface.
- Since we were interested in understanding the formation and diffusion processes at those pressures where that indent in the absorption signal occurs in Figure 25, we also studied the diffusion process in that region. Figures 30 to 33 show the expansion of YbF signal for 14 torr and 17 torr, i.e. just in the decreasing slope and rising slope of the indent respectively. But as already mentioned, the minimum of this indent depends on the distance between probe beam and target when we recorded the data that lead to Figure 25. In both cases we see an intensive absorption signal for the first one two hundred  $\mu\text{s}$  within the first 2 to 4 mm that then decreases rapidly. Afterwards the signal recovers for longer distances, but much less intensive. It seems that the bunch of molecules stays around at particular points for a certain time and then proceeds travelling on. Especially in the case for 17 torr one might think that the cloud of molecules is confined in a certain volume around the target ( $\sim 2$  mm). We will return to that question later on.

So, there is an obvious difference to the process that can be observed at 7.2 torr. For lower pressures the bunch of molecule sticks together while propagating through the cell. The intensity does not decrease very much. But for higher pressures the data reveal a totally different picture. Firstly, the absorption signal decreases much faster. Secondly, the width of the bunch is much smaller, 1-2 mm compared 10 mm in the case of 7.2 torr. And thirdly, the intensity itself is lower,  $\sim 50\%$  to  $75\%$  of the intensity for 12 torr, which is just before the indent).

These differences are likely due to the shorter mean free path length for higher pressure. Thus, the YbF interacts with the buffer more often and cannot propagate through the more dense buffer gas that far. Additionally to that, we guess that due to the higher collision rate and the radical character of YbF those molecules react with  $\text{SF}_6$  further to higher order Yb/F

connections such as  $\text{YbF}_2$  or  $\text{YbF}_3$ , which is in fact stable, but not detected by the probe beam.

- We also studied the diffusion processes for even higher pressures such as 25 torr. In that case the results are quite similar to those for 17 torr. The absorption signal or if we like the bunch of molecules seems to be confined to a certain volume around the target ( $\sim 5$  mm). In that case the maximum intensity is even lower than for 17 torr, although we would have expected a higher one due to Figure . Additionally to that, the data reveals that the propagation of the  $\text{YbF}$  does not seem to be directed towards a certain destination rather than randomly spread within the confining volume. This picture suggests that the higher the pressure, i.e. the lower the mean free path and the higher the collision rate with the buffer, the more undirected the propagation. With a higher collision rate the  $\text{YbF}$  loses more of its primary transferred momentum by the YAG pulses.
- The data on the enclosed DVD contain another expansion study that is not shown in this report. There, we tried to do the same measurements for a very high pressure such as 1 torr, but as already mentioned the Pirani gauge is not quite suitable for pressures above 0.8 torr and so we disbelieve the displayed pressure value of 0.92 torr. It turned out that the pressure was even above 1 atmosphere during this measurement. Nevertheless, these data reveal another picture of the diffusion process since we could observe a bunch of  $\text{YbF}$  propagating through the cell without a tremendous loss in intensity, although we would have expected a confining effect for higher pressures.

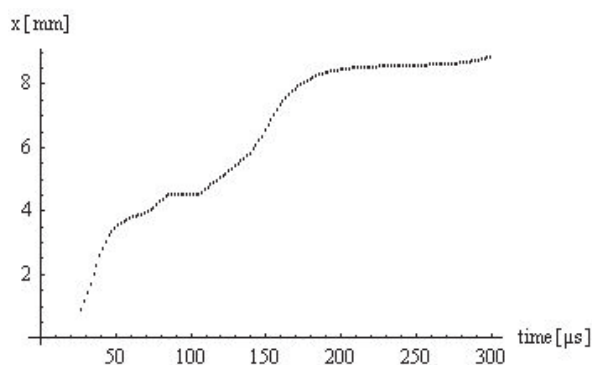


Figure 35: Maximum position versus evolution time at 7.2 torr

## 9.2 One-dimensional diffusion study

Assuming a radially symmetrical density distribution for the bunch of YbF around the x-axis and a maximum in density for  $z = y = 0$  we would like to present a one-dimensional expansion study for the diffusion process. So the following pictures contain cross-sections through Figures 32 and 33 for  $z = y = 0$ . They give an impression how the bunch of molecules is propagating towards the YAG window and allow us to get information about the shape and the size of these bunches in the propagation direction.

What we can see is that the bunches have a more or less Gaussian like shape in the propagation direction. So, we fit a Gaussian profile to these cross-section, an example of which is shown for those at 17 torr. From these cross-sections we can extract the width and the position of the maximum and their time evolution which is shown in Figures 37 and 38 for a particular pressure values we considered in the previous section (17 torr).

At this point we would like to recommend to study the diffusion movies presented on the enclosed DVD. There, we get a more realistic impression of the time evolution of the absorption signal as it travels through the space. Especially for pressures above 12 torr, we can observe a kind of pulsed movement, i.e. the signal seems to stay at a particular position and then to continue its way before its movement apparently gets obstructed again. That is what Figure 37 exactly shows, i.e. a step function for the position of the maximum versus time. We also plotted the width of the bunch versus the evolution time. There we can see particular peaks that can be interpreted in the following way: A peak means that the bunch of molecules dissolves and propagates to another place, where it builds up and dissolves again after a certain time.

A possible explanation for that feature might be again the interaction of the colliding bunch of YbF with the buffer. The entire process can probably be compared to the situation of a ball falling into a container filled with water. If the dimensions of the container are small enough, we observe a quite similar wave feature rather than a propagating 1/r-wave in the case of an infinitely extended container.

Note: The impression might be misleading. It is conspicuous that the bunches always rest at those points, where we have taken the data, i.e. at the grid points, but never in intermediate region, where we interpolated the signal. Thus, this special diffusion feature might be due to the typical structure of our grid (see Figure 27). A closer meshed grid with more points could answer this question, but was not applied in this study.

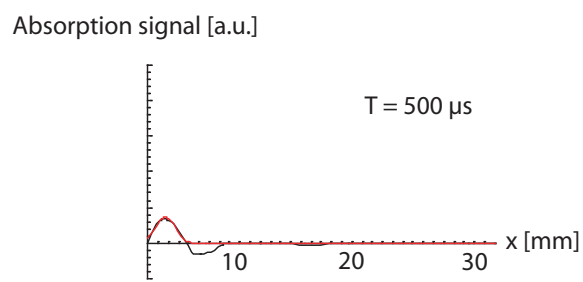
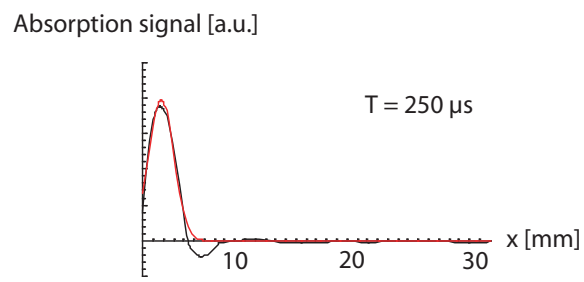
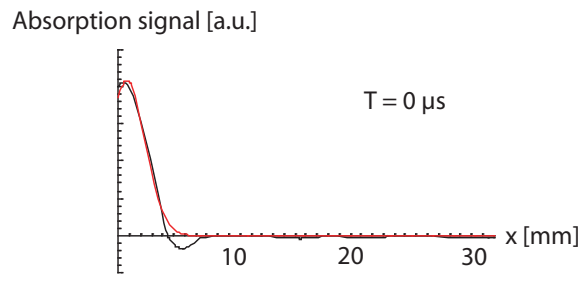


Figure 36: One-dimensional diffusion process at 17 torr

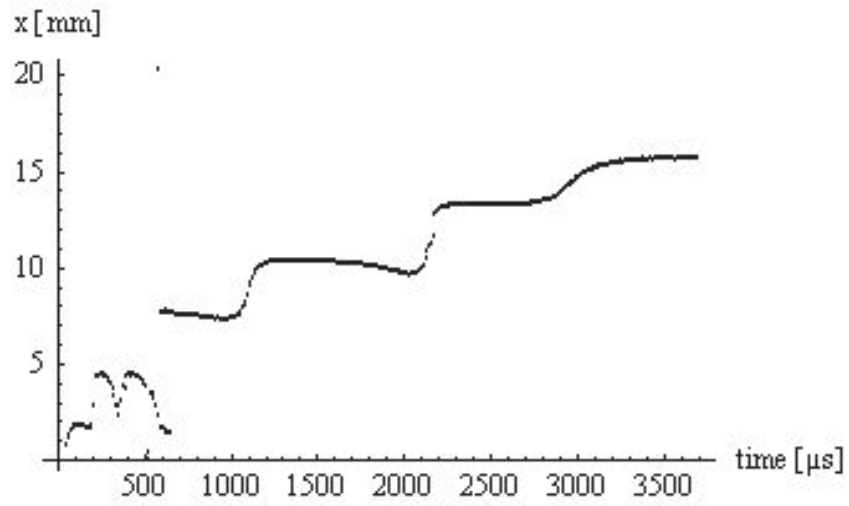


Figure 37: Maximum position versus evolution time at 17 torr

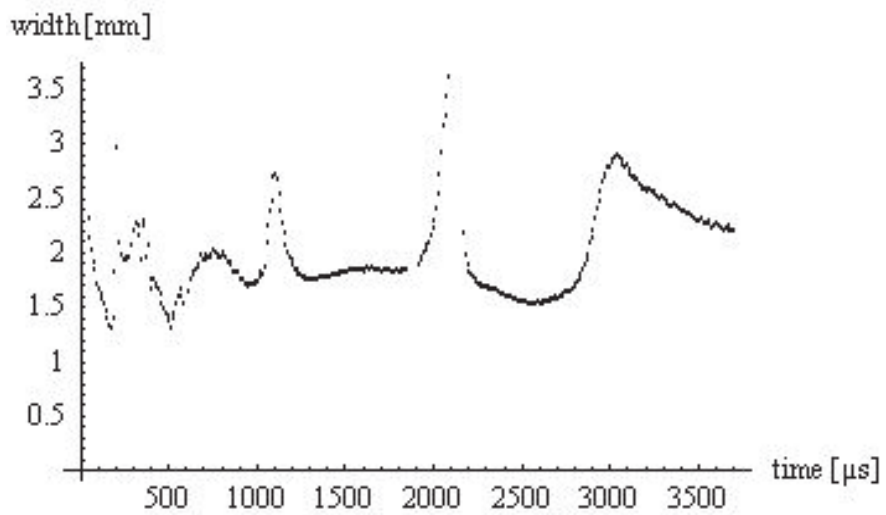


Figure 38: Bunch width versus evolution time at 17 torr

## 10 Production rate of YbF

Since the new approach to a buffer gas cooled source for molecular radicals is intended to provide a higher number of YbF than the current, where Yb is ablated outside the buffer gas chamber and then entrained in a supersonically expanding jet of Ar/SF<sub>6</sub>, the following section presents a fairly simple, but realistic model enabling us to estimate the order of magnitude of the amount of YbF being produced in the ablation cell.

Assuming a static cloud of YbF molecules we consider only its "internal dynamics", i.e. we ignore the production, diffusion and reaction dynamics. This assumption will later on turn out to be justified since the characteristic timescales for these processes are much slower than the timescales for the internal dynamics.

We start out by dealing only with one isotope of YbF, which is acceptable because there is no coupling between the different isotopes, so we can write down separate rate equations for each isotope. We will treat <sup>174</sup>YbF, and suppose that the probe laser is tuned resonant with the Q(0) line. Since there is almost only one transition within the Doppler width of the laser, we use a 3 level model as illustrated in Figure 39:

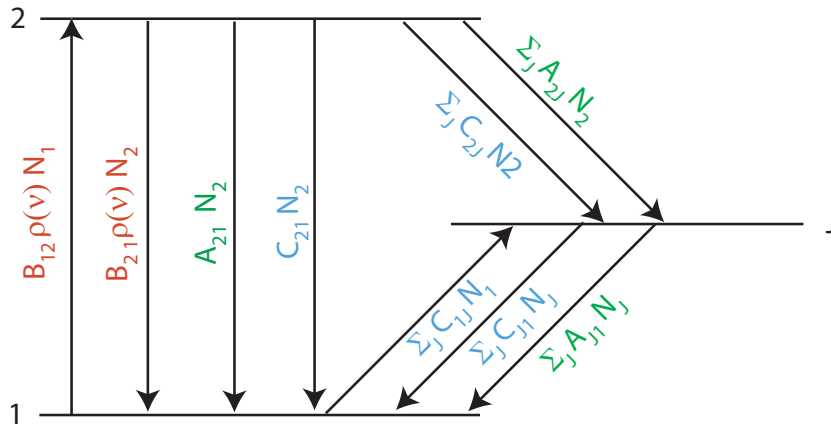


Figure 39: Three level model for internal dynamics of YbF

Level 1 is the ground state of the molecule, and level 2 is the state that is connected to with the laser ( $\nu = 0$ ,  $N = 0$  level of the A state). Level J represents all the other rotational and vibrational levels of the ground electronic state. The A

and B coefficients are the well known Einstein coefficients, and the C coefficients characterize the rates of population transfer due to collisions with the buffer gas. This model does not include a rate for collisional excitation of level 2, because there is never enough energy available in the collision for this process to occur.

If the absorption of the light is small so that we can think of the probe laser intensity as fixed, we can write down a rate equation for  $N_1$ :

$$\begin{aligned} \frac{dN_1}{dt} = & -B_{12}\rho(\nu)N_1 + B_{21}\rho(\nu)N_2 \\ & + A_{21}N_2 + C_{21}N_2 + \sum_J (A_{J1}N_J + C_{J1}N_J - C_{1J}N_1) \end{aligned} \quad (26)$$

Note: A little bit frightening, but not hopeless. Later on it will turn out that one rate is dominating.

The following paragraph considers the relative orders of magnitudes:

**A-coefficients** If  $\Delta\nu_N$  is the natural line width of the transition  $|1\rangle \rightarrow |2\rangle$ , and  $s_{21}$  is the branching ratio, then  $A_{21}$  is given by

$$A_{21} = 2\pi\Delta\nu_N s_{21} \quad (27)$$

For our transition,  $\Delta\nu_N \approx 20$  MHz. We can estimate the branching ratio for our case, because it has already been estimated that for the molecular beam of the current jet beam source the number of photons scattered per molecule is 1.9. This implies a branching ratio of 0.47 ( $\sum_{n=0}^{\infty} 0.47^n = 1.9$ ). This gives an  $A_{21}$  coefficient of  $6 \cdot 10^7 s^{-1}$ .

Furthermore, since  $\sum_J A_{2J}$  represents the rest of the branches, and our branching ratio is basically 0.5, we get the value of this rate also to be  $6 \cdot 10^7 s^{-1}$ .

**Spectral density**  $\rho(\nu)$  If the power in our probe beam is  $P$ , and the radius of the beam is  $R$ , the spectral energy density is

$$\rho(\nu) = 2 \frac{P}{\pi R^2 c} \frac{1}{2\pi\delta\nu_D} \quad (28)$$

where  $\delta\nu_D$  is the doppler width (the dominant broadening mechanism).

For our 1 mW, 1 mm probe beam we get  $\rho(\nu) \simeq 2 \cdot 10^{-16} Jsm^{-3}$ .

$B_{21}\rho(\nu)$  We get  $B_{21}$  from the relation between the A and B coefficients:

$$B_{21} = 2 \frac{c^3}{8\pi\nu^3 h} A_{21} \approx 6 \cdot 10^{20} \quad (29)$$

We find that the stimulated emission rate is very much smaller than the spontaneous emission rate in our case,  $B_{21}\rho(\nu) \approx 1.02 \cdot 10^5$ . This will help to simplify the model.

**Collisions  $C_{mn}$**  We can use some input about collisions between YbF molecules and argon gas because of some measurements using the current supersonic source. There, it was found that the cross-section for a collision between a YbF molecule and an argon atom that removes population from the ground-state is  $8 \pm 1 \cdot 10^{-16} \text{cm}^2$ . So we know the value of  $\sum_J \rho_{1J}$  summed over all relevant levels J.

$$\sum_J C_{1J} = nv \sum_J \rho_{1J} \quad (30)$$

Here, n is the density of the gas atoms and v is the relative speed of the YbF and the gas atoms. We can write n in terms of p, the pressure:

$$n = \frac{p}{k_B T} \quad (31)$$

The relative speed of the YbF and argon is related to the temperature and mass, and is about 300 m/s for typical temperatures. For a pressure of 10 torr, we find the value of  $\sum_J C_{1J}$  to be  $6 \cdot 10^7 \text{s}^{-1}$ .

This leads us to an important conclusion. For our working pressures (above 1 torr), the rate of collisional depopulation of level 1 dominates the rate of photon absorption. The picture we have is one in which collisions between the YbF molecules and the argon atoms maintain the YbF population at equilibrium. A YbF molecule that finds itself in the ground state will occasionally absorb a photon from the probe beam and find itself in the electronically excited state. The population in this state is always small because the rate of spontaneous emission is high compared to the rate of absorption and stimulated emission.

So, our idea is that we do not need to take the rate equation into consideration at all. The YbF should come into equilibrium with the buffer gas in a timescale less than 1 microsecond (for our working pressures). We can then write down the population in the ground state in terms of the total YbF populations  $N_T$ :

$$\frac{N_1}{N_T} = 1 / \sum_{\nu, J} (2J + 1) \cdot \text{Exp}[-(\omega\nu + BJ(J + 1))/k_B T] \quad (32)$$

Here,  $\omega$  and  $B$  are the vibrational and rotational constants respectively. For YbF, these are (in temperature units),  $B = 0.347$  K and  $\omega = 728$  K.

Since  $B/k_B T \ll 1$ , the rotational part of the sum can be done by converting to an integral. The answer is just  $k_B T/B$ . The vibrational part of the sum we can solve numerically. For all temperatures up to 3,000 K the answer lies between 1 and 4.5 (see Figure 40).

$$\begin{aligned} \sum_{\nu, J} (2J + 1) \cdot \text{Exp}[-(\omega\nu + BJ(J + 1))/k_B T] & \quad (33) \\ & = \frac{k_B T}{B} \sum_{\nu} \text{Exp}[-(\omega\nu/k_B T)] \end{aligned}$$

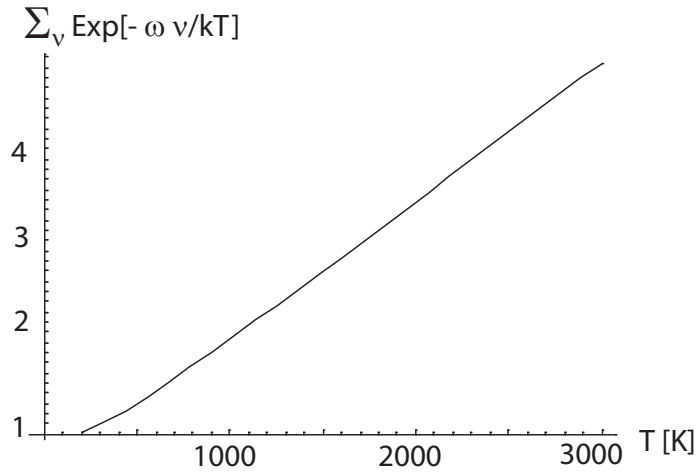


Figure 40: Numerical solution of the vibrational part of the sum above

Now we can think about the absorption of the probe beam. If  $\Delta I$  is the change in the intensity of the probe beam in travelling through a distance  $\Delta x$ , and  $n_1(x)$  is the density of ground-state YbF at the point  $x$ ,

$$\Delta I = -B_{12}\rho(\nu)n_1(x)\frac{hc}{\lambda}\Delta x$$

$$\begin{aligned}
&= -B_{12} \frac{I}{2\pi c \delta\nu_D} n_1(x) \frac{hc}{\lambda} \Delta x \\
&= -A_{21} \frac{\lambda^2}{16\pi^2 \delta\nu_D} I n_1 \Delta x \\
&= -\frac{\lambda^2 \delta\nu_N}{8\pi \delta\nu_D} s_{21} I n_1 \Delta x \\
&= -\sigma I n_1 \Delta x
\end{aligned} \tag{34}$$

So, the intensity after a distance  $x$  is

$$I(x) = I(0) \text{Exp} \left[ -\sigma \int_0^\infty n_1 \Delta x dx \right] \tag{35}$$

where

$$\sigma = \frac{\lambda^2 \delta\nu_N}{8\pi \delta\nu_D} \tag{36}$$

Estimating the natural line width to be 20MHz and the Doppler width to be 1GHz, and a branching ratio of 0.5, we get  $\sigma = 1.2 \cdot 10^{-16} m^2$ .

Writing

$$\chi = \int n_1 \Delta x \tag{37}$$

with the integral running over the whole length where there is absorption, we get

$$\chi = \frac{1}{\sigma} \ln \left[ \frac{I_{in}}{I_{out}} \right] \tag{38}$$

If, at peak absorption, the output intensity is e.g. about 1/5th of the input, then  $\chi = 1.6/\sigma = 1.3 \cdot 10^{16} m^{-2}$ . Since we have measured the absorption as a function of transverse position (assuming cylindrical symmetry) we can estimate the length over which the absorption is significant to be about 5mm, and we get a YbF ground-state density in the cell of about  $2.6 \cdot 10^{18} m^{-3}$ .

We get the same order of magnitude if we consider the Lambert Beer absorption law with de-tuning for our transition  $|1\rangle \rightarrow |2\rangle$ .

$$\Delta I = -\hbar\omega\Gamma_{Ph} \tag{39}$$

whereas the photon scattering rate  $\Gamma_{Ph}$  is given by

$$\Gamma_{Ph} = \gamma\rho_{22} = \frac{\gamma}{2} \frac{S_0}{1 + S_0 + 4\delta^2/\gamma^2} \quad (40)$$

Assuming  $S_0 = \frac{I}{I_{sat}} \ll 1$ , i.e. small saturation, we get

$$\Delta I = -\hbar\omega n \frac{\gamma}{2} \frac{1}{1 + 4\delta^2/\gamma^2} S_0 = -\frac{\hbar\omega n \gamma}{2I_{sat}(1 + 4\delta^2/\gamma^2)} I = -\sigma I \quad (41)$$

with

$$\sigma = \frac{\hbar\omega n \gamma}{2I_{sat}(1 + 4\delta^2/\gamma^2)} = \frac{3}{2\pi} \frac{1}{1 + 4\delta^2/\gamma^2} \lambda^2 \quad (42)$$

In both cases the cross-sections are very similar and provide the same order of magnitude for the YbF ground-state density.

Figure 41 shows the dependence of the order of magnitude for the YbF ground-state density on the ratio  $\frac{I_{in}}{I_{out}}$ :

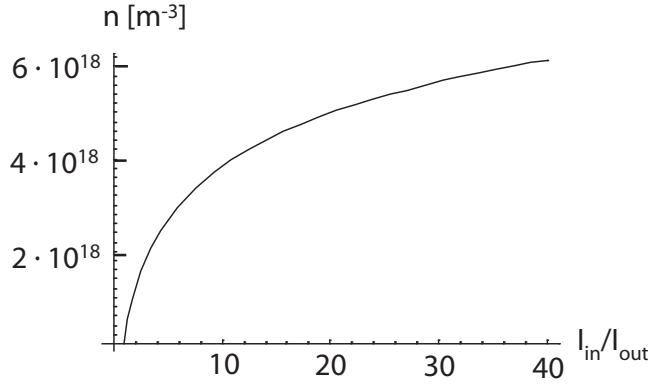


Figure 41: Order of magnitude for the YbF ground-state density versus the ratio  $\frac{I_{in}}{I_{out}}$

Since we have never measured absorption ratios higher than  $\frac{I_{in}}{I_{out}} = 40$ , the density of ground-state molecules always lies within one order of magnitude, i.e. round about  $10^{18} m^{-3}$ .

If we consider all YbF molecules that are in any vibrational or rotational level of the A state, we estimate the density of all YbF molecules to be about 3 orders of magnitude higher than the number above, in total  $10^{21} m^{-3}$ .

# 11 Conclusions and outlook

## 11.1 Conclusions

This study dealt with the production of molecular radicals by laser ablation. The study was performed on YbF, which offers a high sensitivity to the electron's electric dipole moment, which is currently being measured at Imperial College. The study tried to set a start point for a new type of molecule source that differs from that one already used in the edm and decelerator experiment at Imperial College. The new idea was to decouple the formation process of YbF from its expansion, since both processes are strongly correlated in the current technology and might cause some limiting factors on the number of produced molecules. Therefore, the target lifetime and pressure/diffusion studies in chapters 5 to 9 have constituted the bulk of this report. At the end we would like to conclude this study by summarizing some important facts:

- We have studied the ablation process of Yb and it reveals that the translational temperature of the ablated Yb is about 3,000 K.
- The target lifetime was one main point of interest. The most important result of this study is the fact that the target lifetime is longer in this case than it is for the current source. We could observe a decay time of at least 8,000 YAG shots that can be extended to even 30,000 for particular pressures, compared to 5,000 shots for the current technology. This is already an important improvement which might be due to the different types of lasers used in current source and this study respectively.
- We have examined the absorption and, thus, the formation rate of YbF depending on the buffer gas pressure and could observe a strong pressure dependence. There are particular pressure regions where the absorption signal breaks down and then recovers slightly. This feature has not been understood in total so far. A really convincing interpretation for this has yet to be found.
- The study shows the diffusion processes of molecular bunches of YbF for different pressures of the buffer. The conclusion that can be drawn so far is as follows: For lower pressures the bunch of molecules sticks more or less together and propagates nearly without opposition through the cell. The velocity is about 500 m/s.

The higher the pressure the higher the interaction rate with the buffer and thus, it seems that the YbF bunch is gyrating and gets confined in a certain space volume due to the lower mean free path at higher pressures.

- We have estimated the order of magnitude of the number of YbF in the rotational and vibrational ground-state to be about  $10^{18}m^{-3}$ . This looks quite promising for the implementation of a generic, buffer gas cooled source for molecular radicals.

## 11.2 Outlook

As already mentioned above, this study sets a start point for a new type of a generic molecule source. The approach of ablating Yb and producing YbF in a buffer gas environment aims to a buffer gas cooled source. So far, we have not started to work on the cooling process for the produced molecules. But the edm experiments requires molecules in the lowest translational, vibrational and rotational states. For the current jet beam source the supersonic expansion make the molecules in these states. Therefore, the next stage for the new source would be to address the question of how to get the molecules out of the chamber. A quite simple picture might illustrate the new task: Drilling a hole into the chamber and see how much we can get out. But this resembles quite much the current technology.

A totally different approach is the idea of a buffer gas cooled source. By integrating the ablation cell into a cryostat, cold He ( $\sim 4$  K) can be used as buffer gas instead of Ar. One might think of a quite similar idea to that developed and established by J. M Doyle's group at Harvard.

Either a magnetic or an electric guiding system could deliver the produced cooled molecules to an experimental section such the edm machine.

So far the outlook into future times.

## References

- [1] Jun Wang, *Laser and Radiofrequency Spectroscopy of YbF Ground State*. PhD thesis, University of Yale, 1996.
- [2] M.R. Tarbutt et al., *A jet beam source of cold Ybf radicals*. Blackett Laboratory, Imperial College, London, *J. Phys B: At. Mol. Opt. Phys.* **35** (2002) 5013-5022, 2002.
- [3] J.J. Hudson et al., *Measurement of the Electron Electric Dipole Moment Using YbF Molecules*. Sussex Centre for Optical and Atomic Physics, University of Sussex, Brighton, *PRL*: Volume 89, Number 2, 2002.